Composites Part B 224 (2021) 109220

Contents lists available at ScienceDirect

Composites Part B

journal homepage: www.elsevier.com/locate/compositesb

New development of ultra-high-performance concrete (UHPC)

Jiang Du [a], Weina Meng [a,*], Kamal H. Khayat [b], Yi Bao [a], Pengwei Guo [a], Zhenghua Lyu [a], Adi Abu-obeidah [c], Hani Nassif [c], Hao Wang [d]

[a] Department of Civil, Environmental and Ocean Engineering, Stevens Institute of Technology, Hoboken, NJ, USA
[b] Department of Civil, Architectural and Environmental Engineering, Missouri University of Science and Technology, Rolla, MO, USA
[c] Department of Civil and Environmental Engineering, Rutgers, The State University of New Jersey, Piscataway, NJ, USA
[d] Centre for Future Materials, University of Southern Queensland, Queensland, Australia

ARTICLE INFO

Keywords:
Autogenous shrinkage
Design methodologies
Durability
Fresh properties
Mechanical properties
Structural applications
Ultra-high-performance concrete (UHPC)

ABSTRACT

Ultra-high-performance concrete (UHPC) is a type of cement-based composite for new construction and/or restoration of existing structures to extend service life. UHPC features superior workability, mechanical properties, and durability compared with conventional concrete. However, some challenges limit the wider application of UHPC, such as low workability for large-volume production, high autogenous shrinkage, insufficient flexural/tensile properties, and unpredictable durability after concrete cracking. Therefore, this paper reviews the state-of-the-art technologies for developing UHPC mixtures with improved properties. This review covers the following aspects: (1) the existing design methodologies; (2) the typical ingredients (e.g., binders, aggregates, chemical admixtures, and fibers) for preparation of UHPC and the underlying working principals; (3) the technologies for improving and controlling key properties (e.g., workability, autogenous shrinkage, compressive performance, tensile/flexural properties, and durability); and (4) the representative successful applications. This review is expected to advance the fundamental knowledge of UHPC and promote further research and applications of UHPC.

1. Introduction

Ultra-high-performance concrete (UHPC) has been developed for three decades and is considered one of the most promising construction materials for future sustainable and resilient infrastructure [1–5]. Given its low water-to-binder ratio (w/b, 0.15–0.25), high particle packing density (0.825–0.855), high-volume of steel fibers (≥2%, by volume), and proper addition of chemical admixtures, UHPC exhibits good flowability (mini-slump flow ≥160 mm) and high mechanical properties (28-day compressive strength ≥120 MPa [6] and tensile strength ≥5 MPa [7], under standard curing; 28-day compressive strength ≥150 MPa, under steam curing [8]). Due to the use of high-volume fibers, UHPC exhibits strain-hardening behaviors after cracking [9,10]. Additionally, UHPC exhibits superior durability because its matrix is nearly impermeable to carbon dioxide, chloride, sulfate, etc., as shown in Fig. 1 [11–13].

In the past 30 years, UHPC has developed through four stages [14]. Before the 1980s, high-strength concrete could only be produced on lab-scale with vacuum mixing and heat curing [14]. In the early 1980s, micro-defect free cement (MDF) was invented for production of ultra-high-strength concrete with compressive strength over 200 MPa. However, the extremely high material cost and complicated production process restrained its applications [15]. Afterwards, dense silica particle (DSP) cement was invented in Denmark [16]. The DSP cement was designed to improve the particle packing density of concrete and was easier to produce compared with MDF cement. Combining the silica fume, superplasticizer, and pressure curing conditions, the maximum compressive strength of DSP incorporated concrete can reach up to 345 MPa [16]. In the mid-1980s, steel fibers were introduced to overcome the brittleness of this concrete. Finally, slurry infiltrated fiber concrete (SIFCON) was developed, which incorporated up to 20% steel fibers (by volume). The 28-day flexural strength of SIFCON ranged from 25 MPa to 70 MPa [17–19]. However, the SIFCON was not workable, which hindered its wider application.

Thanks to the advancement of superplasticizers in the 1990s, reactive powder concrete (RPC) with superior workability was developed by Richard and Cheyrezy, which is considered the most major milestone in the UHPC development [20]. The RPC was classified into two grades,

* Corresponding author.
E-mail address: wmeng3@stevens.edu (W. Meng).

https://doi.org/10.1016/j.compositesb.2021.109220
Received 12 November 2020; Received in revised form 2 August 2021; Accepted 9 August 2021
Available online 14 August 2021

RPC200 (strength below 200 MPa) and RPC800 (strength from 200 MPa to 800 MPa). Since then, the term "ultra-high-performance concrete (UHPC)" was introduced [21]. Later, the first commercial UHPC was developed based on the recipe of RPC [20], then many other UHPCs were commercialized [22–28]. Some representative commercial UHPC formulations are summarized in Table A of the Appendix. The features of these UHPC mixtures include: (1) extremely low water-to-binder ratio (0.15–0.24), (2) optimized gradation of solid particles for high particle packing density (0.825–0.855), (3) finely grounded quartz sand (d_{max} < 0.6 mm), (4) high cement content (800–1100 kg/m^3) and silica fume content (150–300 kg/m^3), and (5) high steel fiber content (2–5%) [29,30]. However, the initial material cost is still high.

After 2000, instead of pursuing high strength, the focus of the UHPC development switched to reduce its CO_2 emissions and initial materials cost for more eco-friendly and economical UHPC. To this end, various methods have been employed: (1) reduce cement content (<850 kg/m^3) and silica fume content (<200 kg/m^3) by using a high volume of supplementary cementitious materials (SCMs) and fillers [31–35]; (2) reduce binder content (<1200 kg/m^3); (3) replace finely grounded quartz sand by conventional concrete sand or quartz sand [36–39]; (4) reduce fiber content by hybrid fiber systems [40–42]; (5) use standard curing instead of heat curing for lower energy consumption [32,43–45]. The representative mixture designs of the economical and eco-friendly UHPC are summarized in Table B of the Appendix. The performance of these UHPC mixtures is comparable with the commercial ones [31,46]. However, the use of different by-products (e.g., fly ash and rice husk ash) may lead to inconsistent performance [47]. For example, the chemical composition of fly ash highly depends on coal sources and combustion processes which may vary. Furthermore, many power plants have changed the combustion process for environmental benefits, increasing the carbon content in fly ash, which may compromise the properties of UHPC [48]. For this reason, the current application of the economical UHPC is mainly in small quantities, such as connections and joints of bridges [49]. Modern UHPC is still struggling to become a mainstream material for wider applications. While UHPC usually works well on a lab scale, the mixing difficulty significantly increased for large-scale production which might lead to the malfunction of the mixer [47]. Thus, the allowable volume for each batch was restricted. For example, Berry et al. [50] used a pan mixer with a maximum capacity of 0.34 m^3, and Mendonca et al. [51] used a pan mixer with a maximum capacity of 0.45 m^3, but the allowable batch size was limited to 0.1 m^3 which significantly affected the construction efficiency. Besides, due to the low w/b ratio and high cementitious materials content, the typical value of autogenous shrinkage of UHPC is reported over 800 με [52]. Under restrained conditions, there is a high risk of cracking and/or debonding for UHPC structures [53–56]. In addition, while UHPC with high-strength steel fiber shows good ductility and resilience, the high-strength steel fibers account for approximately 35% of the total costs of UHPC which resulted in the high initial cost of UHPC [57]. Thus, it is challenged to reduce the steel fiber content while retaining or further improving flexural/tensile properties. Further, although the intact UHPC has excellent durability, cracks always exist in concrete structures under outer service loads. Attention should also be paid to the durability when some special raw materials were incorporated, such as waste glass and porous sand, which may introduce expansive gel and porosity [58]. In recent years, more researchers have focused on the development of UHPC using new materials and advanced technologies to resolve the associated issues and expand the adoption of this novel class of cementitious composites, while maintaining its high mechanical properties and durability.

This paper comprehensively reviews the new development of UHPC. First, the design methodologies and typical UHPC designs are summarized. Second, the typical ingredients of UHPC are discussed, such as binder materials (e.g., cement, supplementary cementitious materials, and fillers), aggregates (e.g., fine and coarse type), chemical admixture (e.g., HRWR, viscosity modifying admixture, shrinkage reducing agent, and expansive agent), and reinforcing fibers. The unique properties, recommended contents, and underlying mechanisms are elaborated for each ingredient. Third, the state-of-the-art technologies to improve and control the key properties of UHPC are summarized. The key properties include workability, autogenous shrinkage, compressive performance, flexural/tensile properties, and durability. Finally, representative applications of UHPC are introduced.

2. Design methodology

UHPC mixtures are designed to achieve a high particle packing density (Fig. 2) that contributes to low porosity, high mechanical strengths, and impermeability. Anderson and Andreasen model is the most widely used theoretical model to design the UHPC [59] to achieve the maximum packing density of particles involved. However, this method only considered the particles under dry conditions, which may not reflect the real particle packing of UHPC because the influence of water and other liquids are not considered [60]. Therefore, to obtain the "real" maximum particle packing, the wet particle packing density method was introduced [61]. However, the maximum packing density does not always result in the best performance of UHPC, thus the performance-based method was developed. This section introduces

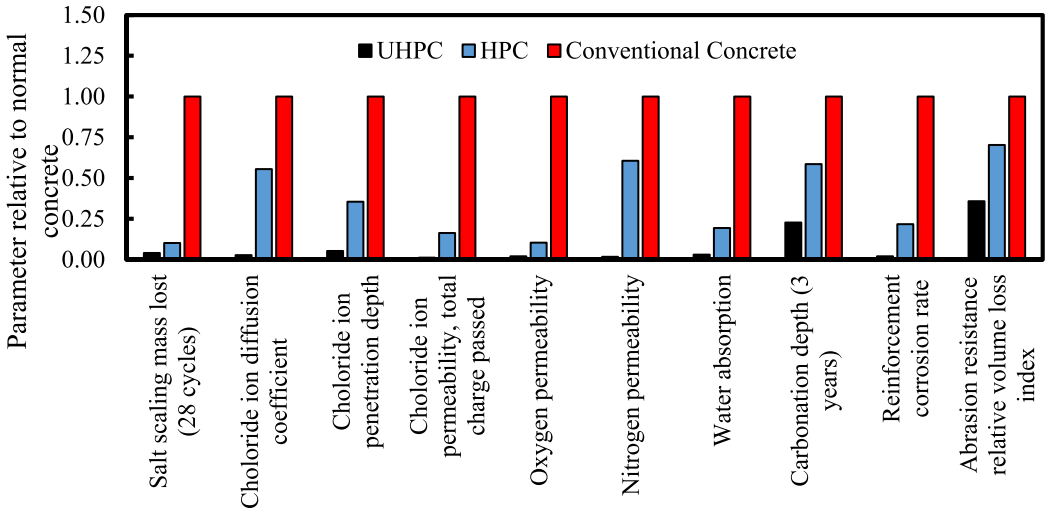

Fig. 1. Evaluation of durability for UHPC compared with HPC and conventional concrete [11].

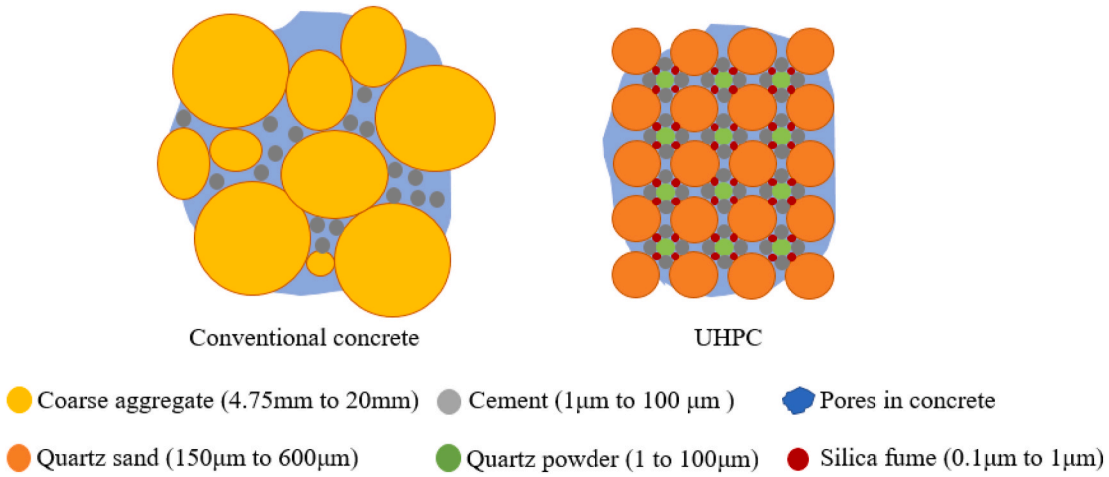

Fig. 2. Two-dimensional schematic particle packing of conventional concrete and UHPC. The UHPC has a higher particle packing density [20].

some useful methods to design UHPC: model-based methods (dry particle packing and wet particle packing methods) and performance-based methods.

2.1. Particle packing model-based methods

2.1.1. Dry particle packing method

For the dry particle packing method, there are two typical models for the mixture design: the discrete model [21,62–64] and the continuous model [65–67]. The continuous model is more preferred in UHPC design because it can achieve a denser particle skeleton as illustrated in Fig. 3.

Fuller [65] and Andersen [66] developed the first continuous model by introducing target particle size distribution P(D). Considering the effect of minimum particle size on particle packing, Funk and Dinger [67] developed the Modified Andreasen & Andersen model and introduced D_{min} as presented in Eq. (1).

$$P(D) = \left(\frac{D^q - D_{min}^q}{D_{max}^q - D_{min}^q}\right) \times 100\% \quad (1)$$

where D_{min} is the minimum particle size (μm) in all materials; D_{min} is the maximum particle size in all materials; q is the distribution modulus.

Brouwers and Radix [69] suggested distribution modulus (q) is in the range of 0–0.25 for concrete with a large amount of cementitious materials [46,70]. For UHPC, the q value was suggested in the range of 0.21–0.25 [71]. Yu et al. [46] developed UHPC mixtures by using the Modified Andreasen & Andersen model. The distribution modulus q was set at 0.23. The optimal volume ratio of each raw material was determined by fitting the composed gradation curve (Fig. 4, dashed line) with the target curve (Fig. 4, solid black line) by using Eq. (2). After confirming the proportion of dry materials, the Puntke test was applied to determine the w/b. Finally, a fixed HRWR content (5% mass of cement) was used to enhance the flowability.

$$RSS = \sum_{i=1}^{n} \left(P_{mix}(D_i^{i+1}) - P_{tar}(D_i^{i+1})\right)^2 \quad (2)$$

where P_{mix} is the composed mixture (black dash line); and the P_{tar} is the target mixture (black solid line) calculated from Eq. (1).

However, the dry particle packing method does not consider the effect of water and HRWR on particle packing. In practice, water and HRWR play significant roles in particle packing and the performance of UHPC [72].

2.1.2. Wet particle packing method

When the fine particles are dry, the high particle friction hinders the increase of packing density [73]. The presence of water can mitigate the friction force. when fine particles are in the saturated or over-saturated state [74], the force can be eliminated. In addition, the addition of HRWR can affect the thickness of the water film on particles and thus the packing density of UHPC [72]. Therefore, a higher particle packing density will be achieved using the wet particle packing model than that determined by the dry packing model, as shown in Fig. 5. A high wet packing density enhances the macro-*meso*-micro pore structures and the compressive strength of UHPC [72].

The wet particle packing model was proposed considering the effect of water and HRWR [61]. To obtain the wet particle packing density, the following procedures should be conducted: (1) set the initial w/b; (2) weigh the water and cementitious materials and mix them; (3) transfer the mixture to a cylinder mold and weigh the amount of paste; (4) calculate the solid concentration (Φ) and void ratio (u) based on Eqs. (3)–(5); (5) repeat the above steps at a lower w/b ratio until the

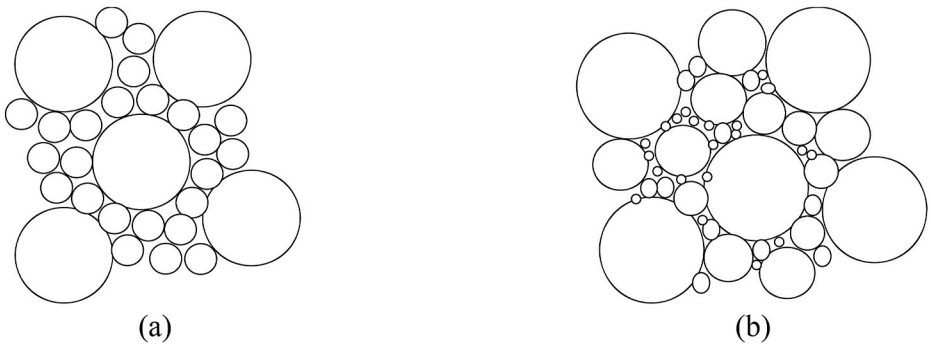

Fig. 3. Two different packing models: (a) binary discrete model, and (b) continuous model [68].

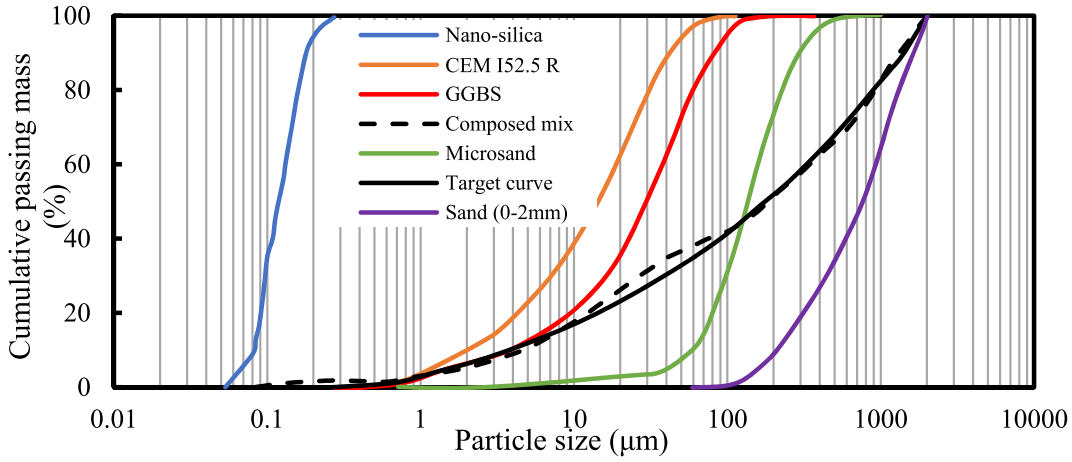

Fig. 4. Particle size distributions of representative dry ingredients, target, and composed curves of the designed UHPC [46].

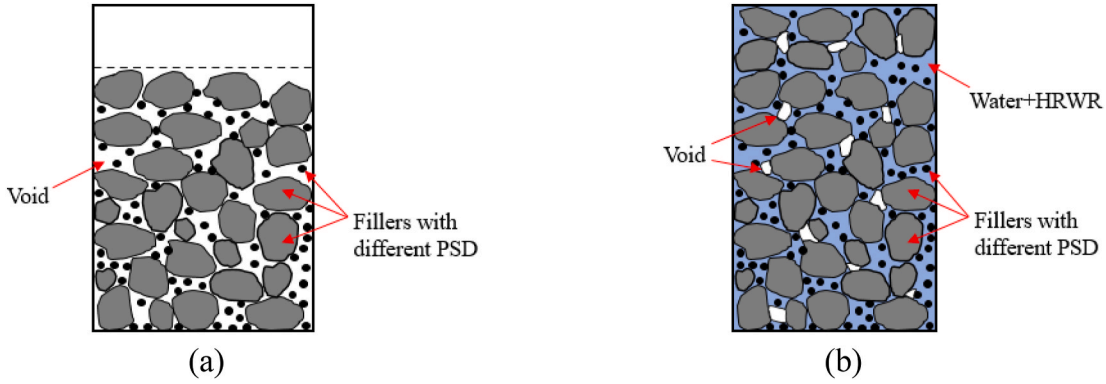

Fig. 5. Particle packing models: (a) dry particle packing model; and (b) wet particle packing model. The wet particle packing model provides a higher packing density [75].

maximum packing density is achieved.

$$V_c = \frac{M}{\rho_w u_w + \rho_\alpha R_\alpha + \rho_\beta R_\beta + \rho_\gamma R_\gamma} \quad (3)$$

$$u = (V - V_c)/V_c \quad (4)$$

$$\varphi = V_c/V \quad (5)$$

where M and V are mass and volume of paste in the cylindrical mold (the mold is of 62 mm diameter × 60 mm height); ρ_w is the density of water, ρ_α, ρ_β and ρ_γ the corresponding solid density of different cementitious materials; R_α, R_β and R_γ are the volumetric ratios of different cementitious materials.

Fig. 6 shows an example of determining the minimum void ratio (u) and the maximum solid concentration (Φ). The optimum w/b can be

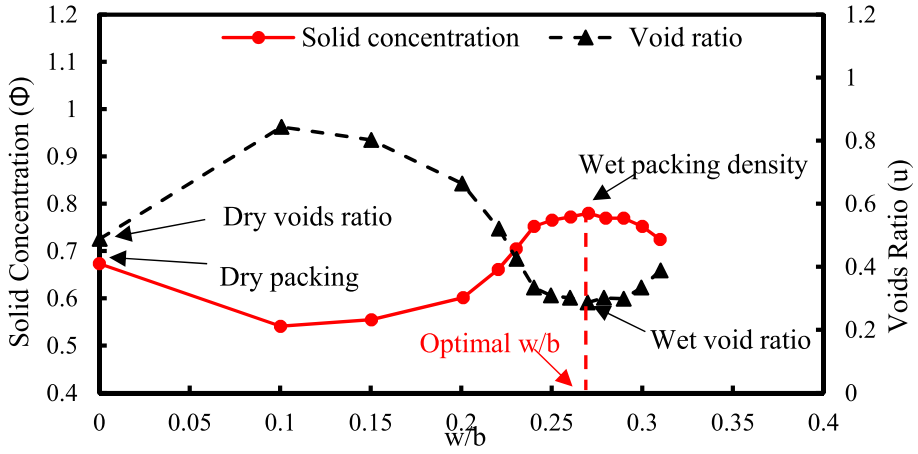

Fig. 6. Trends of solid concentration and void ratio of typical mixtures versus w/b. With this relationship, the optimal w/b for the highest wet particle packing can be determined [60].

determined given the highest wet packing density.

However, the highest particle packing density does not always lead to the expected performance of UHPC. For instance, high particle packing does not ensure the high fire resistance of the UHPC mixture, because a relatively high porosity is preferred to release pore pressure in a high-temperature environment.

2.2. Performance-based method

To design UHPC mixtures in compliance with desired performance for different applications, performance-based methods were proposed [76]. Meng et al. [31] developed a performance-based method to optimize non-proprietary UHPC mixtures. Fig. 7 illustrates the step-by-step optimization process. First, the binder combination has three sub-steps: (i) preliminarily select binder combinations by flow characteristics; (ii) narrow down the binder combinations considering particle packing, flowability, and mechanical properties; and (iii) finalize the binder combinations according to rheology properties including plastic viscosity (μ_p) and yield stress (τ_0). Second, the w/b for paste is determined considering both workability and 28-day compressive strength. Subsequently, the sand gradation, binder-to-sand ratio, and steel fiber content are determined by the modified Andreasen & Andersen model and overall performance. The finalized non-proprietary UHPC mixture is adjusted to satisfy the requirements of the mini-slump and 28-day compressive strength.

The main advantage of the performance-based method is that the mixture design parameters, such as w/b, fiber content, and binder to sand ratio, can be directly and accurately determined based on the relationship established between the variables and the target performance.

3. Typical ingredients of UHPC

This section introduces the characteristics and working principles of typical ingredients in new development of UHPC, including binder materials, aggregates, reinforcing fibers, and chemical admixtures.

3.1. Binder materials

3.1.1. Cement

Depending on the environmental conditions and applications, the types of cement used in conventional concrete include Type I to V and white cement [77] which can all be employed to develop the UHPC. Type III [78] and white cement [14] are the most used types because they can provide fast setting and strength development due to the high C3S content and Blaine fineness. If a high early strength is not mandatory, but a relatively low shrinkage is preferred, Type I cement is alternatively used as its cost and reactivity are relatively low.

3.1.2. Supplementary cementitious materials

Representative SCMs include silica fume, fly ash, slag, glass powder, and rice husk ash, which have been used in UHPC to reduce its cost and carbon footprint and improve properties. Chemically, SCMs feature a high amount of SiO_2 or/and reactive CaO, which can promote cement hydration through pozzolanic and/or hydraulic reactions, especially when the w/b is extremely low. Table 1 summarizes the chemical compositions, physical properties, and typical contents of the most common SCMs used in UHPC. Their effects on workability, mechanical strength, volume stability, and durability are compared with the "Reference mixture" (see Table C in Appendix).

3.1.2.1. Silica fume. Silica fume is a typical but critical constituent for UHPC mixtures, with typical usage ranging from 5% to 25% depending on the volume of the binder. Due to the small particle size, the addition of silica fume (when <10%) improves the particle packing density of UHPC, thus increasing the workability. However, when the content exceeds 10%, the workability may be significantly reduced because the high surface area [79] of silica fume is prone to adsorbing free water and HRWR, which causes particle agglomeration and suppresses the cement reaction [80,81]. Silica fume has a high SiO_2 content (>90%), which provides a seeding effect and pozzolanic effect, promoting cement hydration [82] and thus refines the microstructure of UHPC. Consequently, the use of silica fume normally increases the mechanical strengths of UHPC, and the refinement of pores benefits the durability of UHPC.

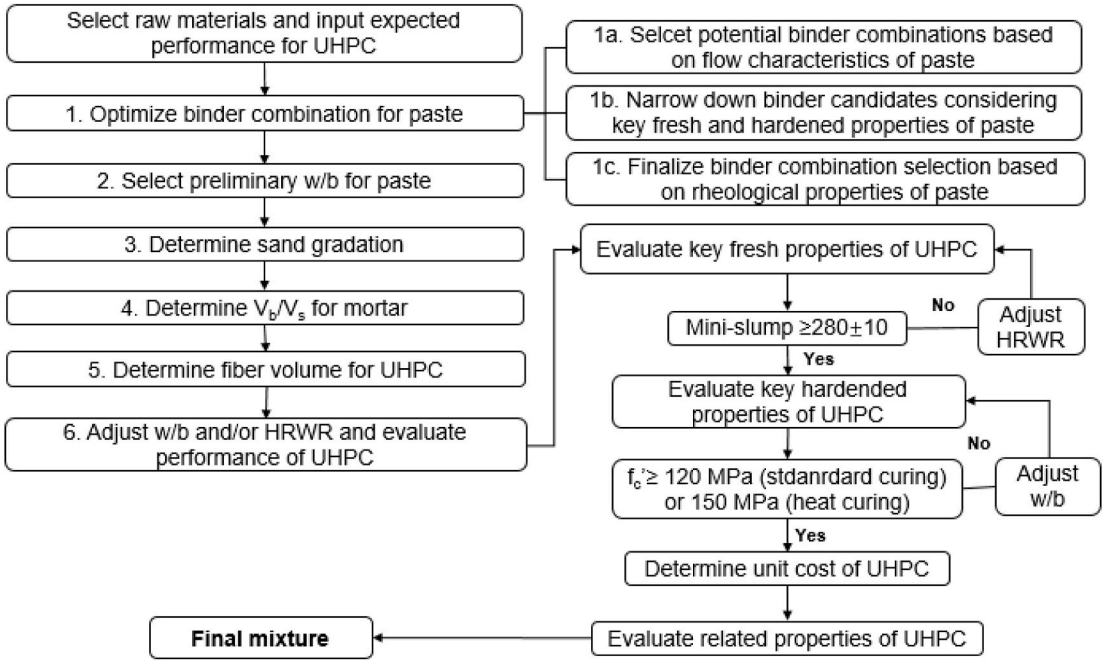

Fig. 7. Flow chart of a performance-based method for designing UHPC mixtures. The left part is the performance-based procedure, and the right part elucidates the performance for each step [31].

Table 1
The summary of supplementary cementitious materials used in UHPC [31–33,46,83–92].

SCMs type		Silica fume	Rice husk ash	Fly ash		Slag	Glass powder
				Type C	Type F		
Chemical composition (%, by mass)	SiO_2	93.9	87.40	36.50	58.40	36.80	73.00
	Al_2O_3	-	0.40	24.80	23.80	9.20	1.50
	Fe_2O_3	0.59	0.30	5.20	4.19	0.76	0.40
	CaO	1.85	0.90	28.10	7.32	37.10	11.30
	MgO	0.27	0.60	5.00	1.11	9.50	1.20
	SO_3	-	0.40	2.50	3.04	0.06	0.00
	LOI	0.30	4.60	0.50	2.13	5.10	0.60
Blaine (m^2/kg)		-	-	465	366	589	Based on application
B.E.T. (m^2/kg)		18500	64700	-	3021	-	
Specific gravity		2.2	2.05	2.70		2.90	
Particle shape factor		-	-	1.20	1.20	1.58	
Typical content (by volume of binder, %)		5-25	20	40-60	10-30	30-50	
Workability		↕	↓	↑	↑	↑	↑
28-day f_c' (MPa)		↕	↑ ~30%	↓ ~10%	↓ ~20%	↕	↑ ~25%
28-day autogenous shrinkage (μm/m)		↕	↓ ~80%	↓ ~25%	↓ ~35%	↓ ~15-65%	↔
Durability		↑	-	↔	↔	↔	↕
Reference		[83, 84]	[33, 85, 86]	[31, 87]	[46, 88, 89]	[31, 90]	[32, 91, 92]

Note: ↑ stands for increases, ↓ stands for lower, ↕ stands for increase or lower, ↔ stands for no significant impact, - stands for limited research, and f_c' stands for compressive strength. These are compared with the reference mixture in Table C in Appendix.

Particle shape factor stands for the degree of deviation from an ideal shape (When the value is closer to 1, the particle shape is closer to spherical).

3.1.2.2. Rice husk ash. Rice husk ash is usually used to partially and/or entirely replace silica fume due to their comparable amount of amorphous silica. The d_{50} of rice husk ash ranges from 5 μm to 20 μm, which is 50–100 times larger than that of silica fume. However, rice husk ash possesses a higher surface area (i.e., 64,700 m^2/kg) than silica fume (i.e., 18,500 m^2/kg) due to its porous structure, making it prone to absorbing more free water and HRWR [93]. As a result, the workability can be significantly reduced with the addition of rice husk ash. Additionally, the high water absorption can cause rice husk ash to absorb the mixing water during the mixing process thus to gradually release to the UHPC matrix during the hydration process, which delays the decrease of internal humidity of pores in UHPC and hence mitigates the autogenous shrinkage, as shown in Fig. 8(a) [33]. As evidenced in Fig. 8(b), the addition of rice husk ash also refines the microstructure, which improves the durability as well as the mechanical performance of UHPC at longer lifespans.

3.1.2.3. Fly ash. Type C and Type F fly ash have been used in development of UHPC [94]. Type C fly ash undergoes both hydraulic and pozzolanic reactions, but Type F fly ash mainly experiences a pozzolanic reaction due to its lack of CaO. Fly ash commonly replaces cement with volume ratios of 40%–60% for Type C and 10%–30% for Type F. As listed in Table 1, the particle shape of fly ash is more spherical than cement, which reduces inter-particle friction, and thus increases the workability [70]. Additionally, d_{50} of fly ash ranges from 30 μm to 50 μm, which is coarser than cement and silica fume. Fly ash can mitigate the self-desiccation-induced shrinkage because more free water is available to retain the relative humidity in the pore solution. Due to the lower hydration reactivity, the replacement of cement with fly ash retards the hydration process [95]. The pozzolanic reaction is slow but can refine the microstructure in long term [96]. The refinement of pores benefits the durability of UHPC. However, due to the high Al_2O_3 content in fly ash, the calcium in the solution is quickly consumed by aluminate to precipitate ettringite on the surface of fly ash, creating a calcium-sink effect. The reduction of calcium concentration reduces the formation of calcium-rich hydration products at early ages. Therefore, the use of fly ash suppresses the hydration process and reduces mechanical strengths

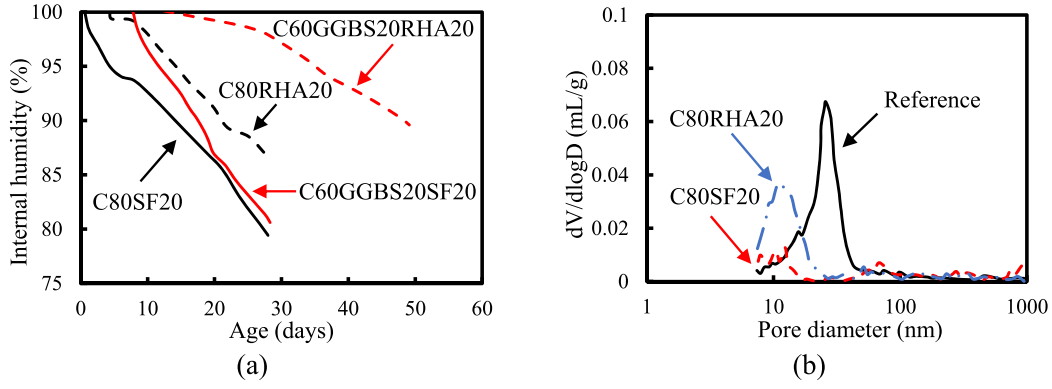

Fig. 8. Comparison of UHPC mixtures with silica fume and with rice husk ash: (a) internal humidity with time [33]; and (b) the pore size distribution [93].

at early ages [97,98].

3.1.2.4. Slag. Depending on the main metal oxides, the slag used in UHPC can include iron slag [31], copper slag [99], and barium slag [100]. As a typical alternative SCMs, slag is usually used to replace cement with a replacement ratio of 30%–60%, depending on the volume of binder. The slag particles have angular shapes (higher shape factor), increasing inter-particle friction and thus reducing the workability of UHPC compared with using the same amount of fly ash. The d_{50} of slag ranges from 30 μm to 50 μm, greater than that of cement, which benefits maintaining a low shrinkage. Similar to the fly ash, the lower hydration reactivity of slag retards the hydration process [99] and tends to refine the microstructure of UHPC [101]). In contrast to fly ash, the slag has a low Al_2O_3 content [97]. The addition of slag in UHPC has less retarding effect on the development of mechanical strengths compared with fly ash [46].

3.1.2.5. Glass powder. Glass powder has been used to replace cement or silica fume of UHPC at a replacement ratio of 10%–50% (by volume of binder), and d_{50} ranges from 1 μm to 20 μm [92]. Among different glass waste sources, soda-lime glass occupies 81% of total glass production and is the main source of glass powder. The smooth surface of glass powder helps reduce inter-particle friction [102]. Additionally, the dense microstructure of glass powder makes it possess a low surface water absorption compared with other types of SCMs. Thus, the addition of glass powder improves workability. In a similar mechanism to the above-mentioned SCMs (i.e., fly ash and slag), the proper use of glass powder refines the pore structure of UHPC [103].

However, when used glass powder is used, a major complication is the potential of an alkali-silicate reaction (ASR). The Na^+ and K^+ ions released by glass powder may increase the pH value of pore solution to be higher than 13, which breaks the chemical bond of siloxane (e.g., ≡ Si–O–Si ≡) of glass and generates ≡ $Si\text{-}O^-$ ions [104]. Then, ≡$Si\text{-}O^-$ ions react with Na^+ and K^+ and produce expansive ASR gel that may cause cracking, as shown in Fig. 9. It was reported that the use of fine particle size glass powder (less than 50 μm) alleviated the ASR. This is because: (1) the pore size in UHPC may accommodate the ASR gel generated by small size glass powder; and (2) fine particle size glass powder can react with calcium hydroxide at early ages to produce C–S–H gel through a pozzolanic reaction, which helps binds alkali ions, densify the microstructure, and improves the crack resistance of the matrix [105].

3.1.3. Fillers

Due to the low w/b in UHPC, the hydration degree of cement at 28 days is usually less than 35% [106], meaning that the majority of cement particles remain unhydrated. The unhydrated cement can be replaced by inert fillers without mitigating the properties of UHPC. The main functions of the filler are to maximize the particle packing density and provide extra sites for the nucleation and growth of hydration products, thus promoting cement hydration degree [107,108]. Depending on the particle size, the fillers are categorized into micro-scale and nano-scale fillers.

3.1.3.1. Micro-scale fillers. Quartz powder is a typical filler used in the production of proprietary UHPC. Quartz is inert and does not participate in cement hydration when temperatures are lower than 150 °C [109]. However, despite the high cost, the International Agency for Research on Cancer (IARC) has reported that it can cause untreatable silicosis [110]. Alternative filler is therefore in demand.

Limestone powder has been proposed as an alternative type of micro filler for UHPC [34,111]. The cement replacement ratio was reported to be up to 50% by volume. The d_{50} of limestone powder ranges from 10 μm to 20 μm, similar to quartz powder. Due to its inert property, spherical shape, and small particle size, the proper addition of limestone powder enhances the workability of UHPC [112]. The use of limestone powder also reduces the autogenous shrinkage and accelerates the hydration reaction [34] due to (1) the filler effect, the limestone powder does not hydrate but provides extra nucleation sites for hydration of cement and/or other reactive particles; (2) the dilution effect, the replacement of cement with limestone powder increases the effective water-to-cement ratio which allows more free water for cement hydration and assists in maintaining the internal relative humidity (IRH) [35]. However, if an excessive amount of limestone powder is used, the hydration peak can be significantly reduced, and the porosity is increased [34]. This is because the overuse of fillers may cause a shortage of reactive materials, limiting the amount of hydration products generated [35].

3.1.3.2. Nano-scale fillers. Inactive nanomaterials, such as nano-$CaCO_3$ [113] and nano-clay (NC), have been introduced to UHPC as nano-scale fillers [114,115]. Due to the very high specific surface area, the additional nucleation and growth sites provided by an appropriate content of nano-scale fillers can effectively promote the hydration reactions and refine the microstructures of the UHPC matrix [116]. Besides, NCs have been found to increase the yield stress and apparent viscosity, as shown in Fig. 10(a). This is because nanoparticles of NCs can fill the gaps between cement particles or pastes agglomerates and the increased physical contact points can lead to the improvement in the rheology of UHPC [117]. However, given a fixed dispersion method, an excessive amount of nano-fillers may cause agglomeration due to inter-particle adhesion via weak forces [118], and thus introduce defects with increased porosity, as shown in Fig. 10(b) [119]. Two main methods have been used for the uniform dispersion: (1) conduct ultra-sonification: the ultrasonic cavitation generates high shear forces that break particle agglomerates into single dispersed particles [120], and (2) add surfactants: the surfactants convert the hydrophobic surface of nanomaterials into a hydrophilic surface for better dispersion in the aqueous phase [121].

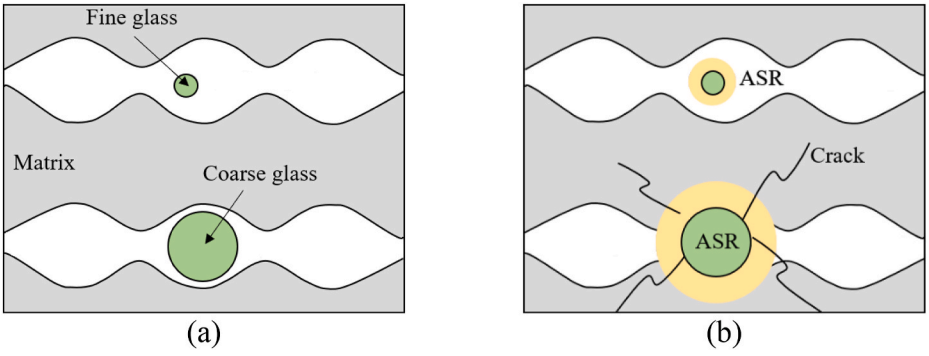

Fig. 9. Illustration of glass particle size on ASR in a cementitious matrix [105]: (a) before any reaction of glass particles, and (b) after chemical reactions of glass particles.

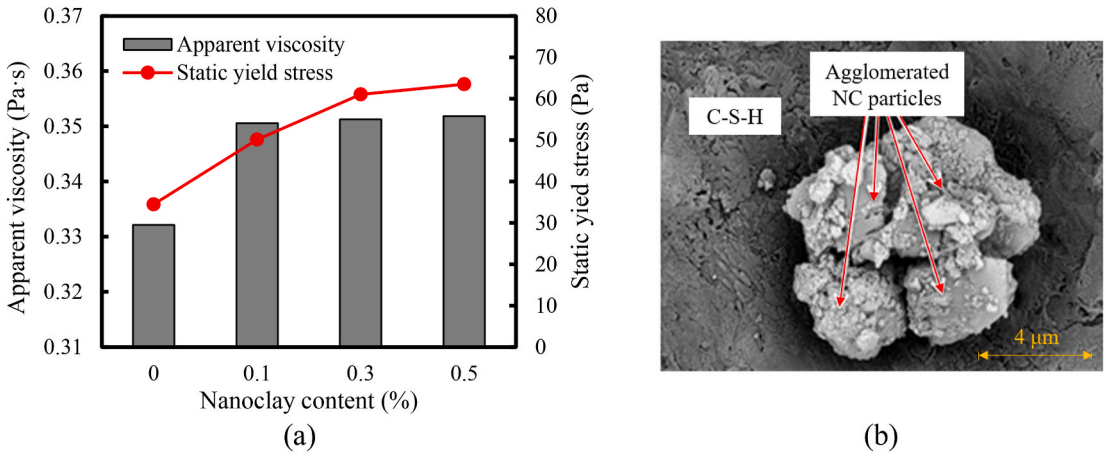

Fig. 10. UHPC with nano-scale fillers: (a) the effect of NC particles on the rheology of cement pastes [122]; and (b) the agglomerated NC particles [123].

3.2. Aggregates

Finely grounded quartz sand with sizes ranging from 150 μm to 600 μm is usually used to prepare UHPC. However, the cost of fine quartz sand is high. Alternative aggregates are therefore proposed for the new development of UHPC. Table 2 summarizes the chemical compositions and physical properties of the alternatives, and their effects on different properties of UHPC. These properties are compared with the "reference mix" (the mixture design is shown in Table C of the Appendix).

3.2.1. Fine aggregates

River sand is the primary fine aggregate used to replace quartz sand [31,36,49]. However, the particle size of river sand ranges from 0 mm to 4.75 mm, with the maximum particle size 5–8 times larger than that of fine quartz sand. Consequently, fully replacing the fine quartz sand with river sand can undermine the particle packing density. To improve the particle packing, finer and more uniformly sized masonry sand (size range: 0–2 mm) was incorporated [31]. However, masonry sand is produced by crushing and grinding coarse aggregates, causing more angular particles than river sand which adversely affects the workability of UHPC [129]. Furthermore, the larger average particle size of river sand and masonry sand compared with quartz sand leads to a weaker interfacial transition zone (ITZ) between sand and UHPC matrix [31,37,49]. Optimization of the particle packing should be conducted to minimize the ITZ.

Limestone sand has a low cost, homogenous composition, abundant reserves, and worldwide availability [130–132]. Yang et al. [133] validated the feasibility of using recycled rock dust in place of fine quartz sand to prepare UHPC. It was reported that the raw cost per unit volume of UHPC was reduced by 40% without sacrificing the workability and mechanical performance [133].

Most recently, the lightweight porous sand has been utilized to produce UHPC, such as lightweight sand [128,134] and volcanic rock sand [126]. The porous structure of this sand allows for internal curing in the UHPC. As shown in Fig. 11, the pre-saturated internal curing agents (i.e., porous sand) hold the curing water during concrete mixing and release the water during concrete hydration. This increases the cement hydration degree and reduces the self-desiccation effect by increasing the IRH [135,136]. Internal curing can provide more effective curing than external moisture curing and help develop UHPC with low shrinkage and high mechanical properties [126–128].

Table 2
The summary of aggregates used in UHPC [31,36,38,55,124–128].

Sand type		Silica sand		Limestone sand/agg.	Basalt sand/agg.	Volcanic rock sand	Lightweight sand
		River sand	Masonry sand				
Chemical composition (%, by mass)	SiO_2	80.3	86.5	0.07	49.62	70.55	57.6
	Al_2O_3	10.5	0.39	0.00	14.93	11.21	19.4
	Fe_2O_3	3.43	1.47	0.02	11.04	4.57	9.6
	CaO	1.72	9.42	56.90	8.22	0.81	3.4
	MgO	1.70	0.00	0.13	7.69	0.06	2.6
	SO_3	1.07	0.00	0.05	0.02	0.06	0.6
	LOI	1.28	0.24	42.73	2.24	2.93	0.0
Specific gravity		2.65	2.64	2.70	2.89-3.05	1.08	1.8
Size range (mm)		0-4.75	0-2.00	0-19.00	0-16.0	0-1.25	0-4.75
Workability		↓	↓	↔	↓	↕	↑
28-day f_c' (MPa)		↓	↓	↓ <5%	↓ <10%	↓ 18~30%	↕ -7~8%
28-day autogenous shrinkage (μm/m)		↓	↓	↔	↓	↓ 5~55%	↓ 30~80%
Durability		↔	↔	↔	-	↑	↑
Reference		[31, 36]	[31]	[124]	[38, 125]	[126, 127]	[53, 128]

Note: ↑ stands for increases, ↓ stands for lower, ↕ stands for increase or lower, ↔ stands for no significant impact, - stands for limited research, and f_c' stands for compressive strength. These are compared with the reference mixture in Table C in Appendix

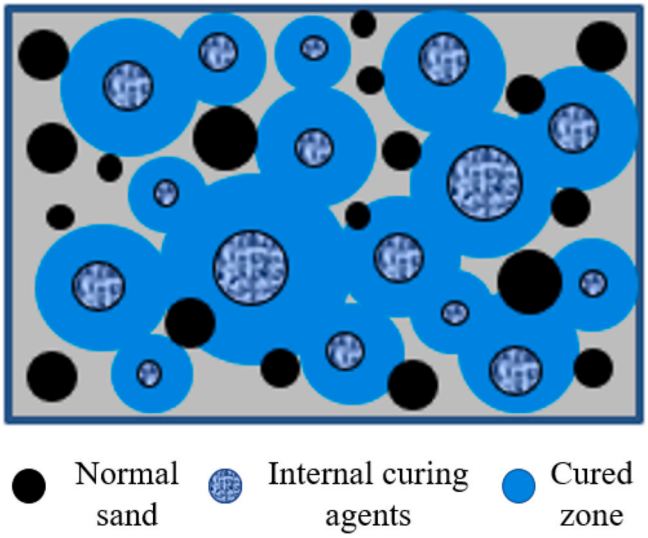

Fig. 11. Schematic illustration of the mechanism of internal curing agents used in UHPC [128].

3.2.2. Coarse aggregates

Basic principles of developing UHPC have been established by Richard and Cheyrezy [20], in which the coarse aggregates (i.e., size greater than 4.75 mm) are generally eliminated. This is attributed to the negative effects of coarse aggregates: (1) the angularity of coarse aggregates significantly reduces the initial packing density of UHPC [38]; (2) the stress concentration at the contact between aggregates leads to weakness in the UHPC matrix [137]; and (3) the ITZ between coarse aggregate and UHPC matrix is weaker than the ITZ between sand and UHPC matrix (Fig. 12) [138].

However, the benefits of using coarse aggregates in the UHPC have been also reported: (1) decreasing the volume of cementitious paste, which increases the elastic modulus and reduces the shrinkage of UHPC, as shown in Fig. 13(a) [139]; and (2) enhancing the penetration impact resistance [140,141]. Due to the low cost, high elastic modulus, and inert property, basalt and limestone have been adopted [38,39]. However, the results show that when the maximum particle size of aggregate was increased from 3 mm to 16 mm, the 28-day compressive and tensile strengths were reduced by 10% and 15%, respectively [38], as shown in Fig. 13(b).

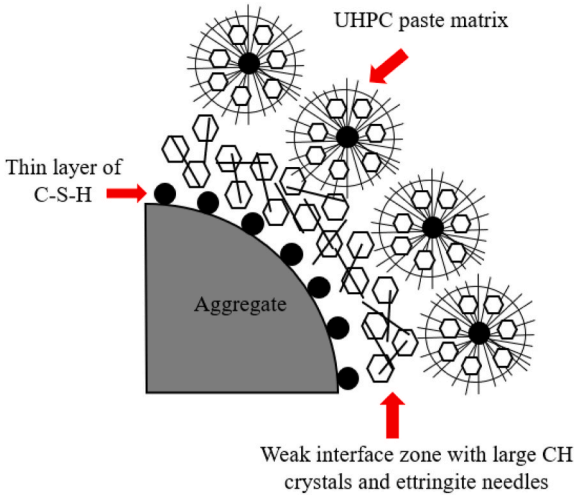

Fig. 12. Schematic illustration of the ITZ between coarse aggregate and UHPC matrix [138].

3.3. Chemical admixtures

Chemical admixtures are used to modify the fresh and/or hardened properties of UHPC [142]. This section reviews the typical chemical admixtures used for UHPC and the underlying mechanisms.

3.3.1. High-range water reducer

High-range water reducer (HRWR) has been used in UHPC to achieve a self-consolidating property [114]. Among different types. the polycarboxylate ethers (PCE) HRWR shows high efficiency in dispersing cement particles [143]. As shown in Fig. 14(a), the PCE head with negative charge is absorbed on the surface of cement particles, and the steric hindrance between the side chains of the absorbed PCE HRWR disperse the cement particles [144]. Attributed to the stereochemistry of the allylether-based HRWR, it is preferred to absorb and disperse silica fume particles. However, the absorbed HRWR on cementitious particles hinders the hydration reaction (Fig. 14(b)), which prolongs the setting time and decreases the mechanical strengths at early ages.

3.3.2. Viscosity modifying admixture

Viscosity modifying admixture (VMA) is composed of water-soluble polymers and can be used to improve the rheological properties of UHPC [146]. The most commonly used VMAs in cement-based materials are cellulose-ether derivatives and polysaccharides from microbial sources such as welan gum [116] and diutan gum [147]. The working mechanisms of VMAs involve the combination of physicochemical effects: (1) Water retention: the long chain of VMA polymers can adsorb free water and swell to increase the viscosity (Fig. 15(a)). (2) Polymer–polymer interaction and entanglement: adjacent VMA polymers can develop attractive forces to form a gel-like network, blocking the motion of water and thus increasing viscosity (Fig. 15(b)). (3) Polymer–particle interaction: the VMA polymers can absorb cement particles, which increases cement particle size, thus strengthening the network and increasing viscosity (Fig. 15(c)).

3.3.3. Shrinkage reducing admixture

Shrinkage reducing admixture (SRA) is composed of organic chemicals [148] - one hydrophilic (polar) head and one hydrophobic (non-polar) tail [149]. The main role of SRA is to reduce the autogenous shrinkage of UHPC by reducing the surface tension in the pore solution of the UHPC matrix. As shown in Fig. 16, the non-polar tail of SRA can absorb the particles at the water-solid interface, and the electrostatic repulsive force between the adjacent polar heads compensates for the shrinkage-induced force and thus reduces shrinkage [150]. Additionally, SRA can absorb air at the water-air interface, retarding water evaporation, thus maintaining the IRH and mitigating the self-desiccation-induced autogenous shrinkage [151].

3.3.4. Expansive agents

Expansive agents are powders that can generate expansive products during the hardening of UHPC. As shown in Fig. 17, the expansive stress compensates for the shrinkage stress, and thus reduces the shrinkage of UHPC. There are three main types of expansive agents: calcium sulfoaluminate-type [152], CaO-type [153], and MgO-type [154]. The calcium sulfoaluminate-type expansive agents produce ettringite in UHPC [155]. However, because ettringite consumes a lot of water, the workability of UHPC can be significantly reduced, and therefore the capacity for reducing shrinkage is limited [156]. Also, ettringite is thermally unstable which is decomposed at 70 °C [157]. Compared with the calcium sulfoaluminate-type, the CaO-type expansive agents need less water to form portlandite which is more stable than ettringite [158]. However, the CaO-type expansive agents react fast at early ages, which prohibits the reduction of shrinkage at later ages. The MgO-type expansive agents have been proposed to compensate shrinkage at later ages [156] because the reaction between MgO-type expansive agents and to produce the $Mg(OH)_2$ is slow.

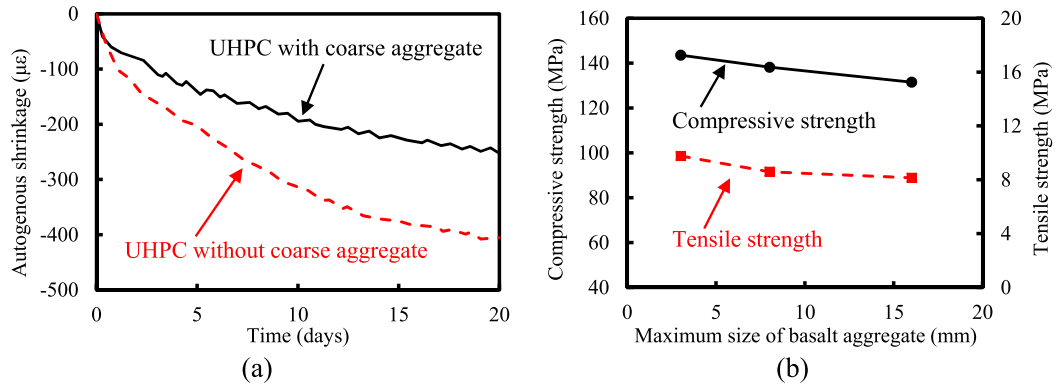

Fig. 13. Effects of coarse aggregate on the performance of a UHPC: (a) the autogenous shrinkage [139]; and (b) the compressive and tensile strengths [38].

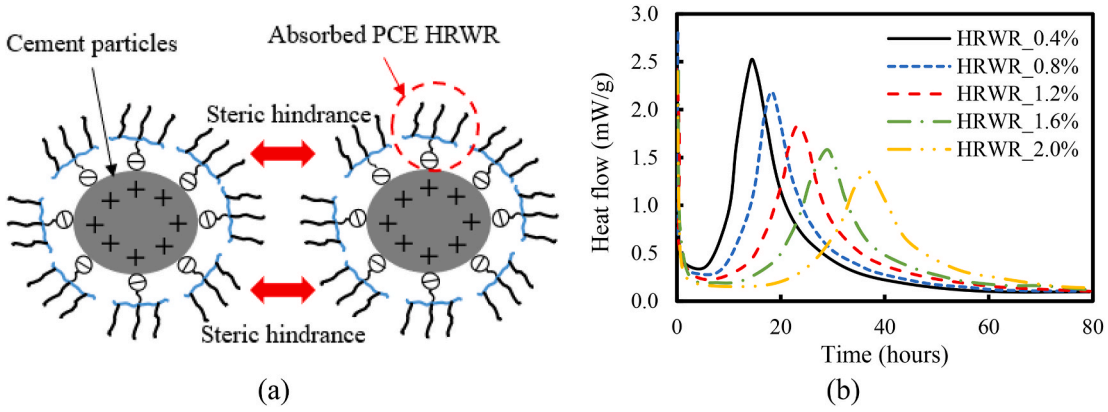

Fig. 14. Effects of PCE HRWR on UHPC: (a) fundamental mechanism of steric repulsion effect [144]; and (b) retarded hydration [145].

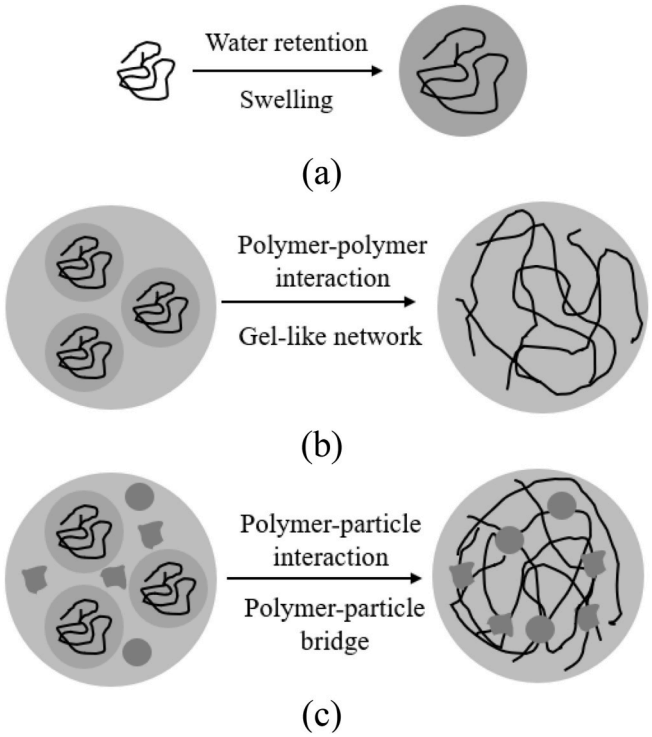

Fig. 15. Schematic illustration of VMAs working mechanisms [146]: (a) water retention; (b) polymer-polymer interaction; and (c) polymer-particle interaction.

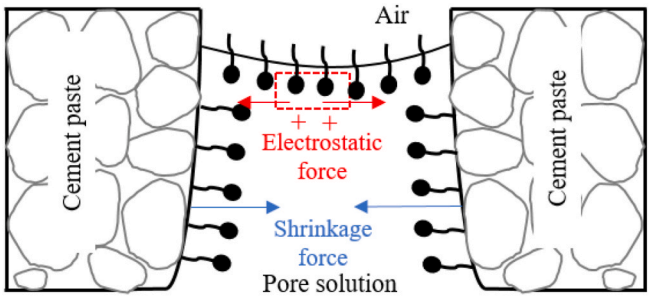

Fig. 16. Working mechanism of the SRA: the shrinkage-induced force is compromised by the electrostatic force between the repellent SRA modules [150].

3.4. Fibers

Fibers are used in UHPC to improve the tensile properties by restraining the initiation and propagation of cracks [160–162]. The characteristics of fibers, including fiber materials (texture), aspect ratio, shape, and surface conditions, significantly influence the properties of UHPC, as shown in Table 3.

3.4.1. Effect of fiber materials

Steel fibers are the most commonly used fibers in UHPC [41]. Meng et al. [41] indicated that as the steel fiber content increased from 0% to 2% (by mass of mixture), the 28-day flexural strength and toughness of UHPC were increased by 120% and 3360%, respectively. However, steel fibers have drawbacks such as (1) high initial cost, (2) corrosion potential [172,173], (3) adverse influence on structure surface finishing

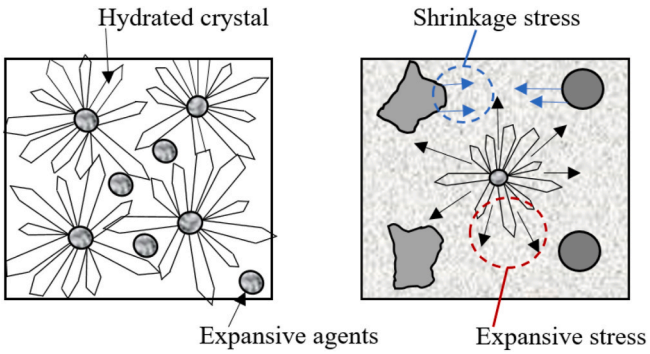

Fig. 17. Working mechanism of expansive agents: the expansive stress compensates shrinkage induced stress [159].

[174], and (4) high density (add dead load).

To overcome the drawbacks of steel fibers, glass fibers with similar tensile strengths have been used [166]. However, the flexural strength of UHPC with 2% glass fibers is reduced by 25% compared to that of UHPC with 2% steel fibers [166]. Alternatively, synthetic fibers such as polyethylene (PE) fibers have been applied. However, the hydrophobic surface of synthetic fiber leads to a porous ITZ between fiber and matrix, which may improve the tensile strain capacity (ductility) by introducing multi-cracking patterns with delayed growth of localized major cracks [175] but compromises the tensile/flexural strength [169]. On the contrary, mineral fibers (e.g., basalt fiber) have similar chemical compositions to the UHPC matrix, generating a strong chemical bond and achieving higher cracking stress [176]. However, the ductility is compromised because cracks initiated due to the rupture of fibers rather than being pulled out of the matrix [177], the crack propagates quickly, which leads to failure of the UHPC.

Along with enhancing tensile/flexural properties, some fibers made with special materials can add beneficial functions [178–183] to the UHPC. For instance, due to the excellent electrical conductivity of carbon, self-sensing UHPC has been developed by adding carbon nanofibers [184]. As shown in Fig. 18(a), the tensile (bending) process gradually generated cracks in the UHPC matrix, and the cracks affected the conductive pathway and increased the electrical impedance. Therefore, the stress-strain curve of the UHPC was satisfactorily monitored by measuring the fractional change in impedance. In addition, materials

Table 3
The summary of fibers used in UHPC [41,163–171].

Fiber type	Steel fiber	Carbon fiber	Glass fiber	Cellulose fiber	Mineral fiber	Synthetic fiber		
					Basalt	PVA	PP	PE
Length (mm)	13	0.05-0.2	13	Depend on the different type (jute, flax, etc.)	12	12	13	19
Diameter (μm)	200	0.1	18		18	100	22	23
Density (kg/m^3)	7800	2000	2600		2800	1300	910	960
Tensile strength (GPa)	1-3	30	2		2.8-4.8	1.23	0.4	3.25
Elastic modulus (GPa)	203	240	52-87		86-90	29.5	3.7	113
Recommended ratio (by volume of mixture, %)	2.0-3.0	0.3-0.5	1.5	< 1.0	0.5	0.5	1.0	1.0
Workability	↓	↓	↓	↓	-	↓	↓	↓
28-day f_c' (MPa)	↑ 5~10%	↓ 5~15%	↓ 5%	↔	↓ 15%	↑ 5%	↓ 15%	↓ 5%
28-day f_f' (MPa)	↑ 5~8%	↑ 10%	↓ 20%	↑ 30% [a]	↑ 3% [b]	↑ 10%	-	↓ 15% [b]
28-day toughness (J)	↑ 5~20%	-	-	↑	↓ 70% [c]	↑ 13%	-	↑ 45% [c]
28-day autogenous shrinkage (μm/m)	↓ 6~15%	-	-	↓ 30% [a]	-	↓ 35%	-	-
Reference	[41, 163, 164]	[165]	[166]	[167, 168]	[169]	[41]	[170]	[171]

Note: f_c' stands for compressive strength, f_f' stands for flexural strength, a stand for 3-day stem curing results, b stands for the 28-day tensile strength, c stands for 28-day tensile strain capacity. The mixtures reinforced by different types of fibers are compared with the UHPC mixture with 2% steel fibers in corresponding papers.

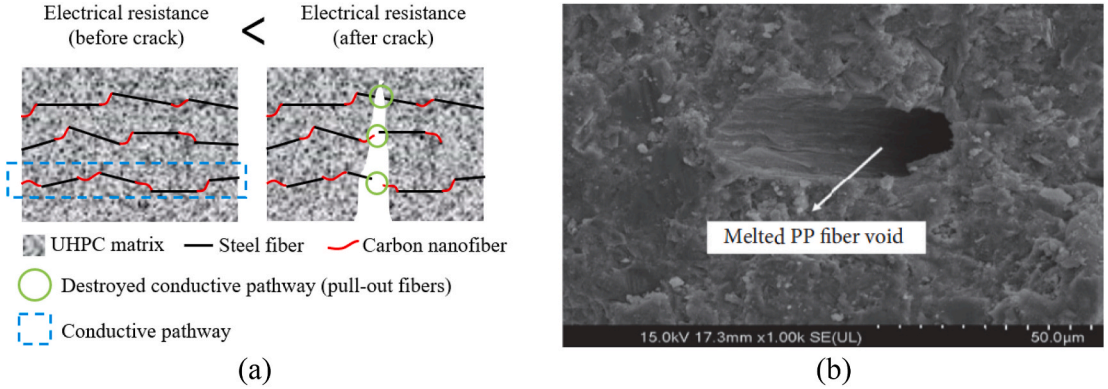

Fig. 18. Mechanisms of multifunctionality of UHPC: (a) self-sensing property due to the use of carbon fibers [184]; and (b) fire-resistance property due to the use of polypropylene fibers [185].

with low melting temperatures such as polypropylene fibers have been used to develop fire-resistance UHPC [185]. When concrete is exposed to elevated temperatures, the melted fibers create channels to alleviate internal vapor pressure and prevent explosive spalling, as shown in Fig. 18(b).

3.4.2. Effect of fiber aspect ratio

The aspect ratio is the ratio between fiber length (L_f) and fiber diameter (D_f) [186]. In most cases, steel fibers with a higher aspect ratio provide better flexural performance (e.g., flexural strength, deflection capacity, and toughness) [57,187]. This is because the reinforcing fibers with a higher aspect ratio have a larger effective fiber-matrix bond area, and thus provide better post-cracking behavior [188]. Yoo et al. found that when the volume of steel fibers was fixed at 2%, an increase in the fiber aspect ratio from 65 to 97.5 increased the flexural strength and toughness of UHPC by 40% and 105%, respectively [57]. Moreover, the number of cracks in UHPC with steel fiber ($L_f/D_f = 97.5$) increased by 125%, and the average crack spacing was reduced by 45%.

3.4.3. Effect of fiber shape

Many shapes of metallic fibers include straight, hooked, corrugated, and twisted [40,41,163] have been used in the UHPC. In particular, the deformed fibers show better performance in enhancing the tensile/-flexural properties of UHPC [189,190]. Fig. 19 summarized the load-slip curves of different shaped steel fibers [191]. For straight fibers, the debonding and friction at the fiber-matrix interface govern the pull-fiber behaviors [192]. For deformed fibers, additional resistance can be provided by the mechanical anchorage/interlock [40]. After the elastic stage (before A1, A2, and A3), different shapes caused different load-slip responses. For the straight fiber, the peak load (B1) was followed by debonding (B1–C1). Then, the fiber was pulled out from the matrix under friction (C1–S) [192]. For the hooked fiber, a steady region (C3-D3) with a constant load was observed after the pull-out load dropped from the peak, which can be attributed to the mechanical anchorage/interlock provided by the hooked end [193]. Finally, the fibers were pulled out from the matrix under friction (D3-S). For the corrugated fiber, multiple steady regions were observed (C2 and D2), because the curved shape led to straightening processes that can carry sustained loads [191].

Researchers have quantitatively evaluated the effect of fiber shape on fiber-matrix bond strength [40,194]. The bond strengths of corrugated and hooked fibers were 200% and 600% higher than that of straight fibers. The flexural strengths of UHPC with corrugated fibers and hooked fibers were 5% and 20% greater than that of UHPC with straight fibers. The bond strength between the UHPC matrix and twisted triangular fibers was 40% higher than that of straight circular fibers. As a result, the tensile strength of UHPC with twisted triangular fibers was 35% greater than that of UHPC with straight circular fibers.

3.4.4. Effect of fiber surface condition

Other than using deforming the fibers, applying treatment to roughen the fiber surface can also improve the fiber-matrix bond [195–199]. Several treatment methods have been developed, including using chemical solutions immersion [194], sandpaper [200], and cold gas plasma [201]. Based on the quantitative evaluation by atomic force microscope images, after 6 h of immersion in an ethyl-enediaminetetraacetic acid solution, the roughness of steel fibers was increased by 290%, as shown in Fig. 20(a) and (b) [194]. Therefore, the tensile strength and strain capacity of UHPC with the roughened steel fibers were increased by 15% and 16%, compared with those of UHPC with untreated steel fibers, as shown in Fig. 20(c).

4. Improve and control the key properties of UHPC

This section addresses the solutions to the challenges related to the workability, autogenous shrinkage, mechanical property, and durability of UHPC, as identified in Section 1.

4.1. Control workability

To facilitate the construction and ensure homogeneity and dense microstructure of UHPC, the workability must be well controlled. If the workability is too high, high-density materials (e.g., steel fibers) will segregate [202] and low-density materials (e.g., synthetic fibers and lightweight sand) will float upward; if the workability is too low, UHPC cannot be self-consolidated, and the dense microstructure required for UHPC cannot be achieved. The methods for adjusting the workability are introduced below.

4.1.1. Improve flowability by regulating hydration

As mentioned in the introduction, the flowability of UHPC depreciates quickly during large-scale field construction, especially at elevated temperatures. This problem is mainly attributed to the initial hydration of cementitious materials, in which the tricalcium aluminate

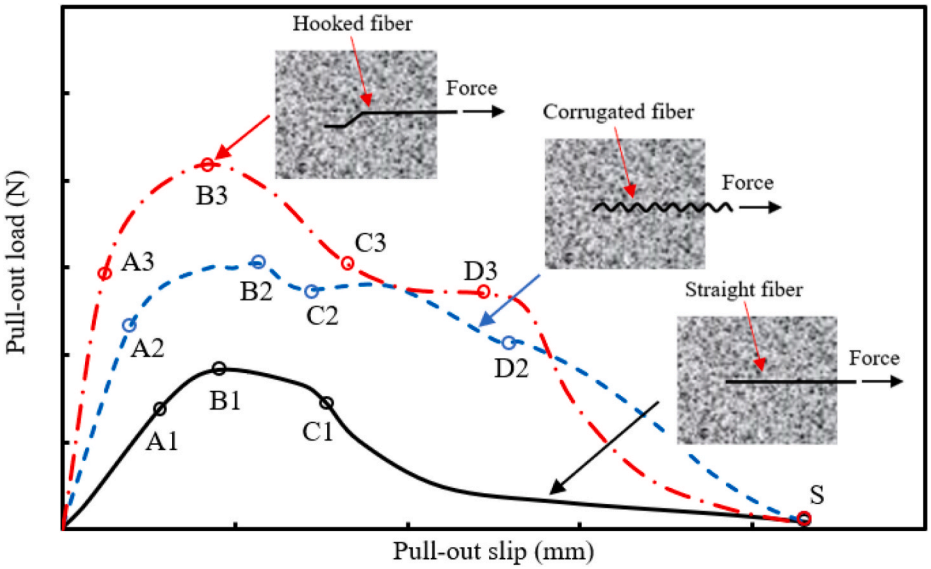

Fig. 19. Comparison of the typical pull-out load-slip curves of different shaped steel fibers.

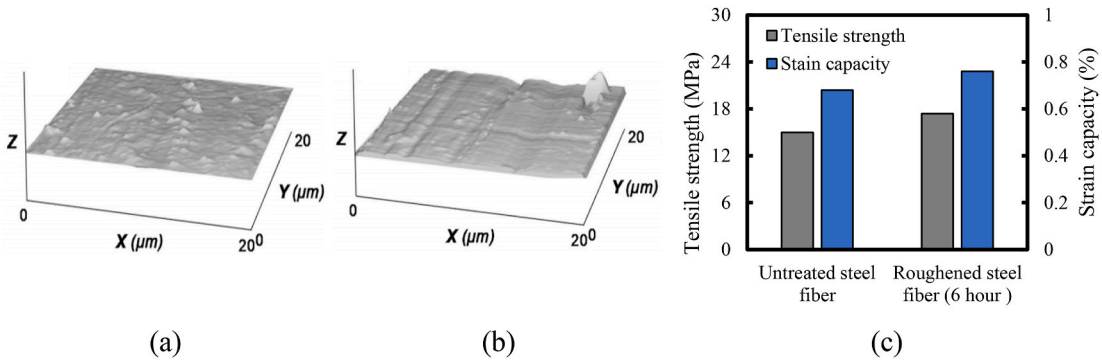

Fig. 20. Effect of surface roughness of steel fibers and tensile properties [194]: (a) atomic force microscope image of untreated steel fibers surface; (b) image of roughened steel fibers surface (6-h immersion); and (c) results of tensile properties of UHPC with different roughness of fibers.

(C_3A) and gypsum in cement react with water and generate a large amount of ettringite that increases the connections and interparticle frictions [203]. Worse still, higher temperatures can increase the dissolution of C_3A and gypsum in water, accelerating the initial hydration and exacerbating the reduction of workability. Therefore, delay or reduce the rate of hydration is key to improve the flowability of UHPC.

4.1.1.1. Physical control of early-age hydration. Because the dissolution rate of C_3A, gypsum, and other ions for the hydration reaction significantly reduces with a decrease in temperature [203], one of the main methods to slow down the early-age C_3A reaction is to reduce the material temperature. To this end, some researchers partially replaced the mixing water with crushed ice. Xie et al. [204] found that when 50% of fresh water was replaced with crushed ice, the temperature of cement paste was reduced from 25 °C to 1.2 °C (Fig. 21(a)) and as shown in Fig. 21(b), when the mixing temperature was reduced from 30 °C to 10 °C, the rate of hydration heat was significantly reduced in the first 50 min, and thus benefits the workability.

4.1.1.2. Chemical control of early-age hydration. Another method is to use high volume SCMs and/or inert fillers to replace the cement and/or silica fume in UHPC [9–11]. The effect of SCMs and inert fillers on hydration reactions is introduced in Section 3.1. Yang et al. [205] found that, as the replacement ratio of slag was increased from 0% to 50% (by mass of cement), the mini-slump spread of UHPC was increased from 260 mm to 310 mm (by 20%) and the dormant period was extended from 2.6 h to 8 h, as shown in Fig. 22. The underlying mechanism is that the replacement of cement by slag significantly reduces the reactive C_3A content in the UHPC.

4.1.2. Control rheology by adjusting chemical admixtures

The rheological properties of the suspension must be controlled to prevent inhomogeneity (Fig. 23) [10]. Meng et al. used VMA for the rheology control [10,206]. It was found that for UHPC with 2% steel fibers, the plastic viscosity of the suspending mortar should be adjusted to around 52 Pa s (optimum value) to obtain the best fiber uniformity. However, the optimum plastic viscosity is dependent on the type and content of fibers. For example, for UHPC with 1% and 3% steel fibers, the optimal plastic viscosity was 36 Pa s and 66 Pa s, respectively [206].

4.2. Reduce autogenous shrinkage

The autogenous shrinkage of cementitious materials is attributed to the internal self-desiccation and chemical shrinkage during the hardening [207]. The typical value for autogenous shrinkage of UHPC is larger than 800 με [52], which has a high cracking potential [53–56]. Reduction of autogenous shrinkage, especially at the early age, is necessary. Fundamentally, four mechanisms control the development of autogenous shrinkage: (1) degree of hydration, (2) reduction rate of IRH, (3) restraint of volume change, and (4) internal forces for compensating shrinkage-induced tension. Based on different mechanisms, autogenous shrinkage mitigation strategies have been summarized in Table 4 and elaborated in the following.

4.2.1. Reduce chemical shrinkage by regulating hydration reaction

Chemical shrinkage due to cement hydration is the main contributor to autogenous shrinkage of UHPC [215]. Compared with cement, SCMs have lower calcium content and hydraulic reactivity, which hinder the hydration process of UHPC and reduce autogenous shrinkage. The

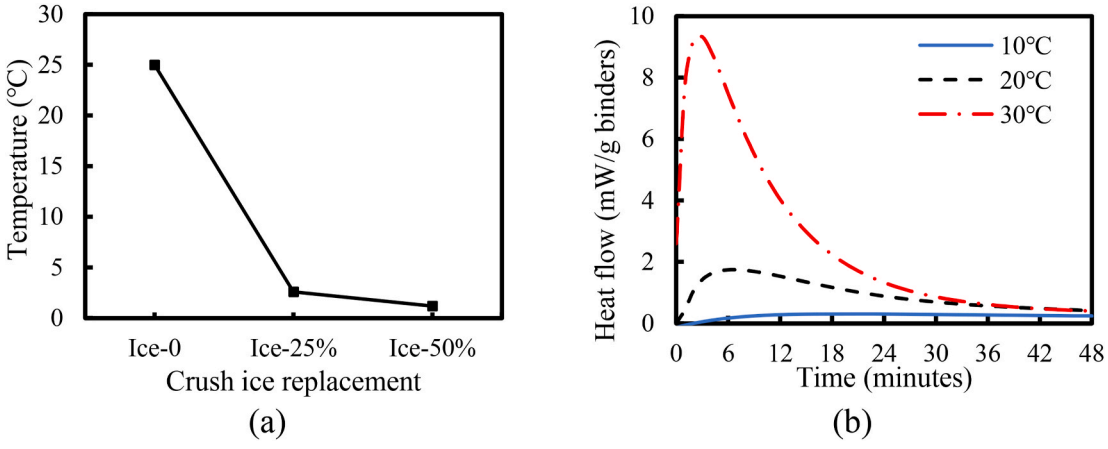

Fig. 21. Physical control: (a) effect of ice replacement on temperature reduction [204]; (b) hydration heat flow of cement paste (w/b = 0.3) at different temperatures (preliminary results).

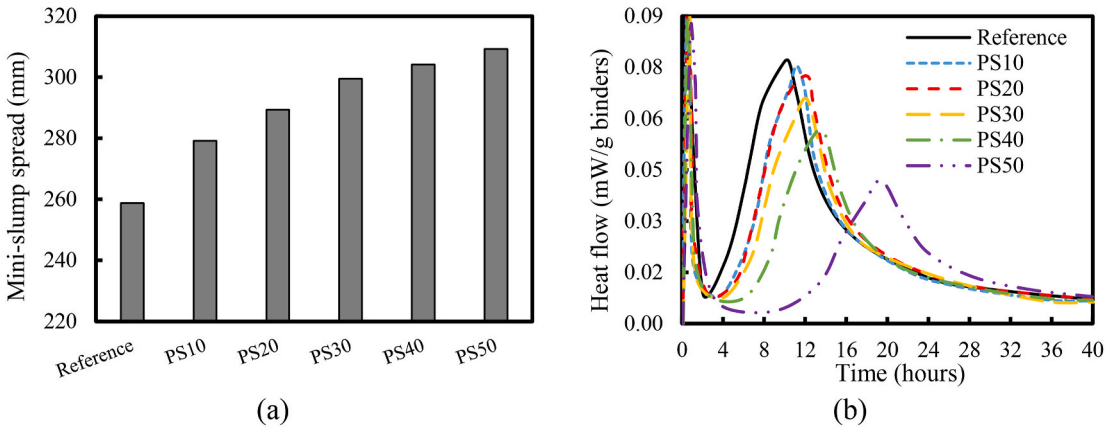

Fig. 22. Chemical control using SCMs [205]: (a) the mini-slump spread; and (b) hydration heat.

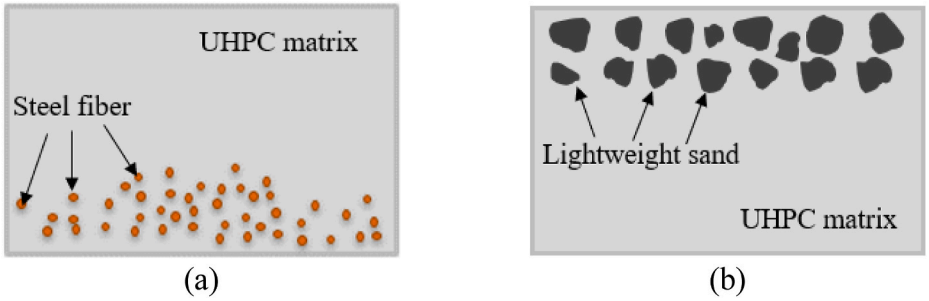

Fig. 23. Inhomogeneity of UHPC with a low viscosity [10]: (a) segregation of steel fibers; and (b) floating of lightweight sand.

Table 4
Summary of strategies to mitigate autogenous shrinkage.

Mechanism	Mitigation method	Recommended content (%)	Mitigation rate (%)	Reference
Degree of cement hydration	Fly ash	20–40[a]	18–24	[31,208]
	Slag	30–60[a]	15–20	[31,208]
	Rice husk ash	100[b]	45–75	[33,209]
	Limestone	20–60[c]	10–30	[35,210]
Reduction rate of internal relative humidity	Superabsorbent polymer	≤0.5[c]	80	[211]
	Cellulose fibers	0.06[d]	35	[168]
	Lightweight sand	25–50[e]	35	[128]
	Porous pumice	30[e]	60	[127]
Restraint degree for volume change	Aggregates	30	40	[139]
	Reinforced fiber	1–3	20–55	[40]
Introduction of internal forces to compensate shrinkage-induced tension	Shrinkage reducing admixture	≤3[c]	45–60	[212, 213]
	Expansive agent	–	15–55	[212, 214]

Note: a by volume of binder, b by volume of silica fume, c by mass of cement, d by volume of mixture, e by volume of sand, - stands for the recommended value is uncertain which is highly related with the type of EA, SRA stands for shrinkage reducing agent, and SAP stands for superabsorbent polymer.

replacement of cement and/or silica fume with less reactive SCMs or inert fillers can regulate the hydration reaction and reduce the autogenous shrinkage. For instance, Kang et al. [35] found that, as the limestone replacement ratio was increased from 0 to 50% (by mass of cement), the 28-day autogenous shrinkage of UHPC was reduced from 818 με to 550 με (by 32%). Ghafari et al. [208] found that, as the silica fume was fully replaced by fly ash or slag, the 28-day autogenous shrinkages of UHPC were reduced by approximately 15%. It is noteworthy that the ability of rice husk ash to mitigate the autogenous shrinkage is stronger than other alternatives due to the porous structure which provides an internal curing effect to reduce the drop of IRH in UHPC [33].

4.2.2. *Reduce self-desiccation by increasing internal relative humidity*

Self-desiccation occurs due to the reduction of IRH. Internal curing agents can be used to maintain the IRH by gradually releasing internal curing water [216]. Different types of internal curing agents have been applied to UHPC, such as superabsorbent polymer (SAP) [217], porous fine aggerate [127,128], and cellulose fibers [168].

4.2.2.1. Superabsorbent polymer. SAP is a type of polymer with a cross-linked surface that can absorb water by an osmotic pressure effect [218–221]. Liu et al. [222] found that, as the SAP content increased to 0.6% (by mass of binders), the 7-day IRH was increased from 76% to 90%, and the 7-day autogenous shrinkage was reduced from 610 με to 189 με (by 70%), as shown in Fig. 24.

However, as the SAP content increased to 0.6%, the 91-day compressive strength of UHPC was reduced from 121 MPa to 111 MPa (by 8%). The negative effect of the SAP addition on strength development was also reported by other researchers [211,223]. The strength reduction is mainly due to the formation of voids after the water desorption from SAP, as shown in Fig. 25 [211]. The voids can increase the porosity of the UHPC matrix and become weak zones.

4.2.2.2. Porous sand. Porous sand such as coral sand, expanded shale sand, and recycled concrete sand can also provide internal curing and has advantages over SAP [218], such as high stability and maintained mechanical strength. The absorption capacity of porous sand is between 10% and 20% [127,128]. Meng and Khayat [128] found that as the

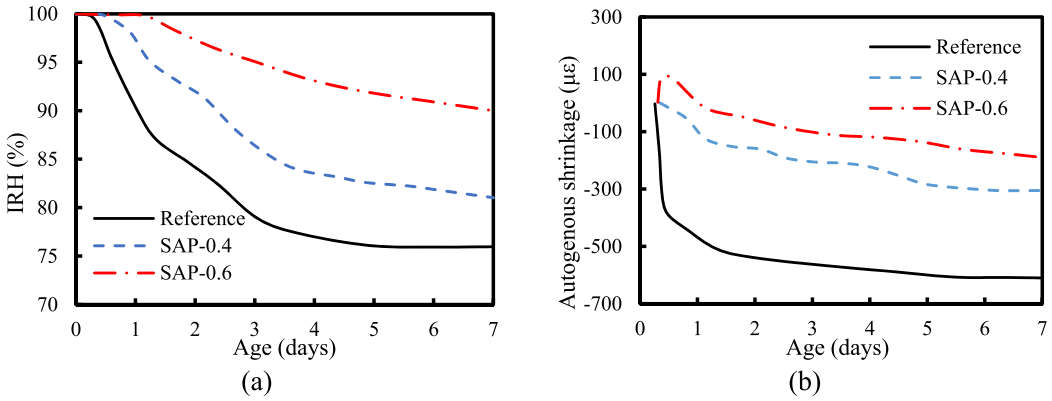

Fig. 24. Experimental results of the effect of SAP on (a) IRH; and (b) autogenous shrinkage [222].

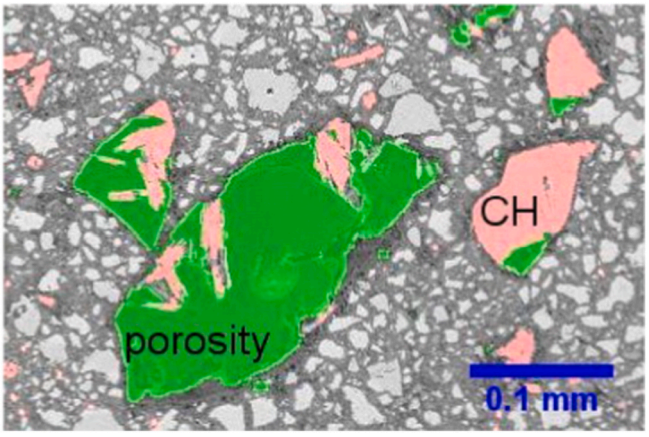

Fig. 25. Detail of SAP voids in UHPC matrix [211]. Note: green color indicates porosity caused by SAP, and pink color indicates CH.

concentration of pre-saturated porous sand (i.e., expanded shale sand) increased from 0% to 75% (by mass of river sand), the 7-day IRH was increased from 83% to 92%, and the 28-day autogenous shrinkage was reduced from 490 με to 197 με (by 60%), as shown in Fig. 26.

As shown in Fig. 27, proper incorporation (≤25%) of pre-saturated porous sand promotes cement hydration that produces hydration products to fill the pores, which reduces porosity, densifies the microstructure, and strengthens the ITZ. However, excessive porous sand increased porosity and reduced the strength of UHPC [10]. A vacuum saturated method has been proposed to retain the IRH for a longer time, which may help minimize the use of porous sand [224].

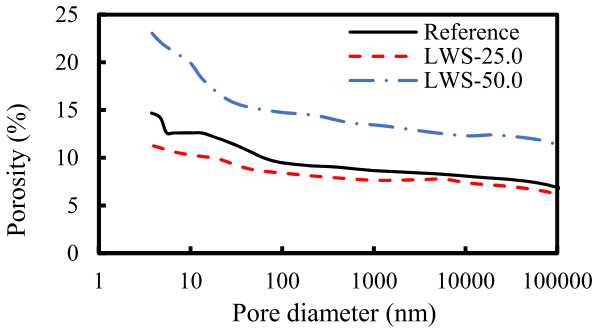

Fig. 27. Effect of the LWS content on the porosity of UHPC after hydrating for 28 days [128].

4.2.2.3. Cellulose fiber. Cellulose fibers have been used as internal curing agents due to the meso-porous structure and high water absorption rate [225]. As shown in Fig. 28(a), the slow water release rate of cellulose fiber at high relative humidity levels (>70%) is advantageous for UHPC because of longer internal curing, and thus benefits the autogenous shrinkage reduction, as shown in Fig. 28(b).

4.2.3. Restrain volume change

Shrinkage can be reduced by providing internal restraints and/or reinforcement such as fibers and aggregates [156]. The mechanism and effects of aggregates on autogenous shrinkage reduction are elucidated in Section 3.2. Reinforcing fibers such as steel fibers can help maintain the volume, resist shrinkage stress, and reduce autogenous shrinkage of UHPC [156]. The effectiveness of the fibers is dependent on fiber

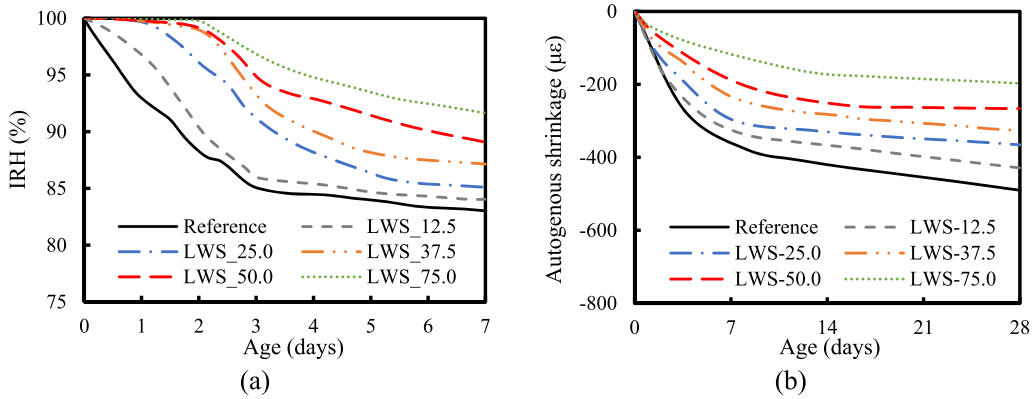

Fig. 26. Results of lightweight sand content on (a) internal relative humidity; (b) autogenous shrinkage. The Figures are adopted from Ref. [128].

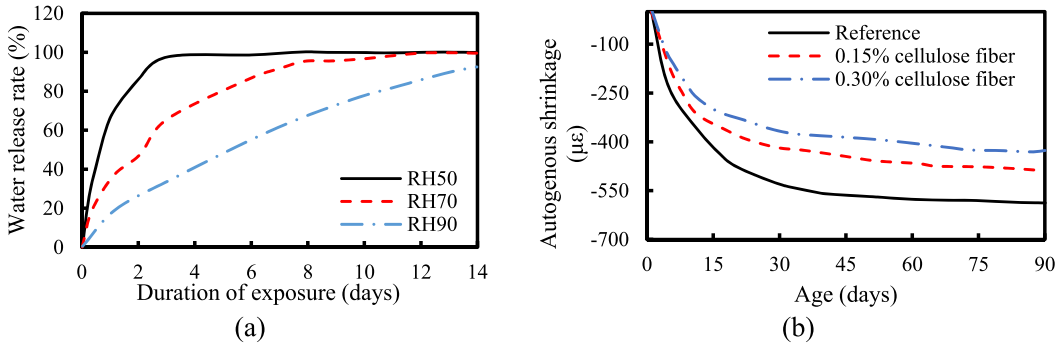

Fig. 28. Effects of cellulose fibers on autogenous shrinkage of UHPC [226]: (a) the water release rate; and (b) the autogenous shrinkage of UHPC with cellulose fibers.

characteristics. For example, as the amount of straight steel fiber was increased from 0% to 3% (by volume), the 72-h autogenous shrinkage was decreased by 50%, as shown in Fig. 29(a) [40]. Given the mechanical interlock effect, the incorporation of deformed fibers can further improve the transferring of shrinkage-induced stress and reduce the autogenous shrinkage. As shown in Fig. 29(b), when straight steel fibers were changed to hooked steel fibers, the 72-h autogenous shrinkage was further decreased by 25%.

4.2.4. Introduce internal forces

4.2.4.1. Induce expansive force. Using expansive agents to induce an expansive force can compensate for the shrinkage in UHPC (Fig. 30(a)) [156]. The mechanism and different types of expansive agents are introduced in Section 3.3.4. However, the 28-day compressive strength of UHPC can be slightly reduced by introducing the expansive agent, as illustrated in Fig. 30(b). The expansive products (e.g., ettringite and portlandite) densify the microstructure of UHPC at early ages, but the water consumed by expansive agents reduces the hydration degree of cement.

4.2.4.2. Induce repulsive force. During cement hydration, the capillary stress is increased due to the surface tension of pore solution [156], thus causing shrinkage. SRA reduces the surface tension by introducing repulsive forces between particles, as detailed in Section 3.3.2. Su et al. [212] found that as the SRA content was increased from 0 to 2% (by mass of cement), the 7-day autogenous shrinkage of UHPC was reduced by 45% (Fig. 31(a)). However, as shown in Fig. 31(b), the use of SRA compromised the mechanical strength of UHPC. This can be attributed to: (1) the SRA is adsorbed on the water-solid (air) interface and generates "organic molecular film" that hinders hydration reaction [213, 228]; and (2) the admixture reduces the alkali contents in the pore solution, which retards the dissolution of C_3S [229]. To mitigate the negative effects, Soliman and Nehdi [230] suggested combining the use of wollastonite microfiber.

4.3. Improve compressive performance

Generally, UHPC has excellent compressive strength due to the low porosity and refined microstructure [231]. In case further improvement of the compressive strength is needed, efforts can be focused on (1) reducing the porosity, and (2) densifying the hydration products.

4.3.1. Reduce porosity

4.3.1.1. Improve particle packing density. Improving particle packing density leads to smaller voids in the matrix and creates more contact points among particles, thus improving the compressive strength of UHPC [232]. Reducing w/b and optimizing the gradation of particles are the typical ways to increase the particle packing. As shown in Fig. 32(a), when the cement content increased from 30% to 100% (by mass of binder), the packing density and compressive strength of UHPC increased and then decreased. The maximum packing density and compressive strength were simultaneously reached when the cement content was 80% [233]. Meanwhile, as shown in Fig. 32(b), when the binder systems were fixed, use glass sand with optimized size also benefits the particle packing, and thus the compressive strength of UHPC [91].

4.3.1.2. Promote hydration reaction. The promotion of cement hydration generates more hydration products, which refine the microstructure of UHPC. According to the Power's model [234], the ultimate hydration degree of a typical UHPC with w/b between 0.20 and 0.22 ranges from 47% to 52%. The unhydrated cement particles can be replaced by fillers

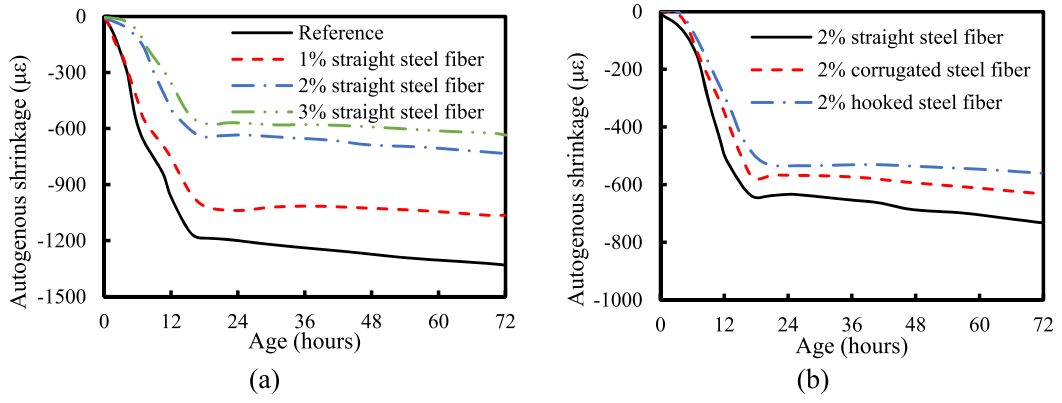

Fig. 29. Results of autogenous shrinkage of UHPC [40]: (a) effect of steel fiber content; and (b) effect of steel fiber shape.

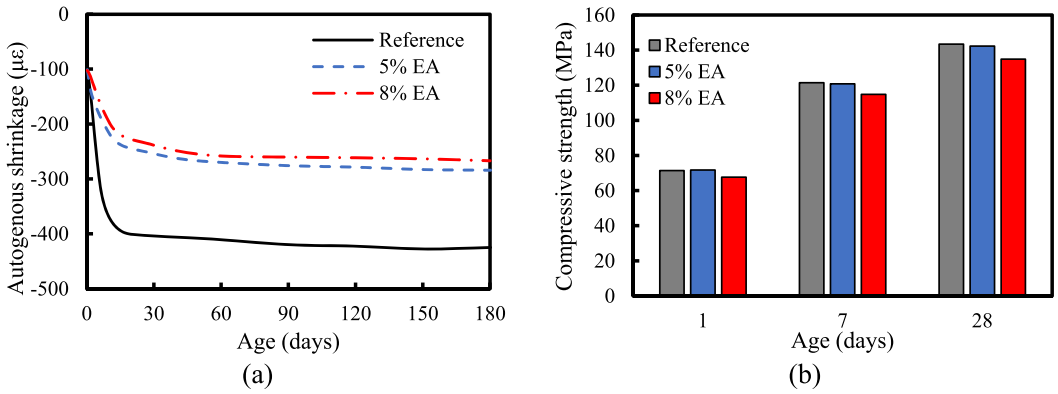

Fig. 30. Results of expansive agent (EA) on (a) autogenous shrinkage and (b) compressive strength of UHPC. The figures are adopted from Ref. [227].

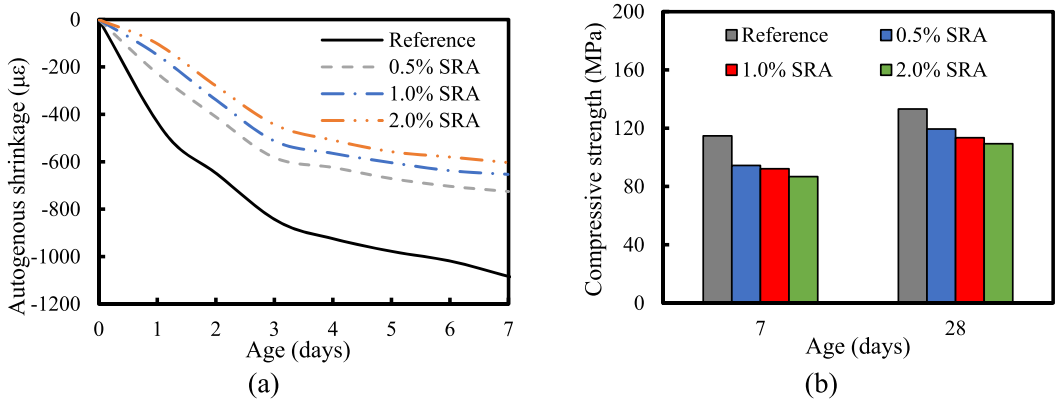

Fig. 31. Results of SRA on (a) autogenous shrinkage, and (b) compressive strength of UHPC (by mass of cement, %) (w/b = 0.2). The figures are adapted from Ref. [212].

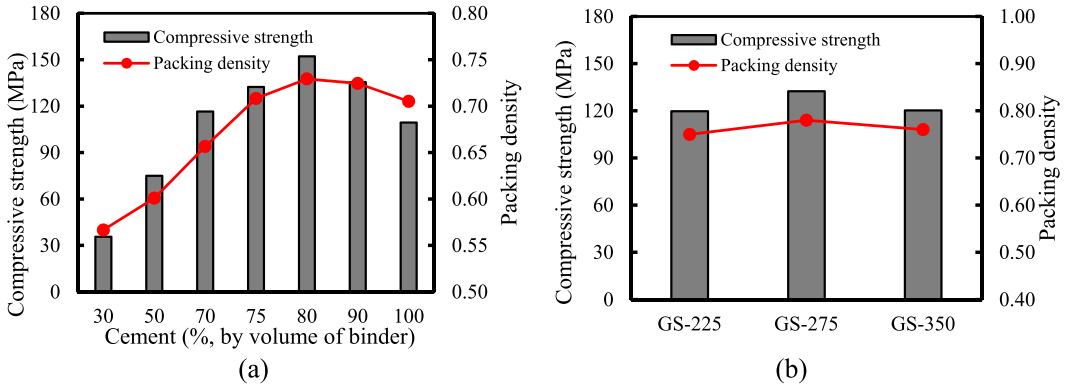

Fig. 32. The relationship between initial packing density and compressive strength: (a) packing density variation by adjusting binder combinations [233]; and (b) packing density variation by adjusting sand gradation [91]. Note: GS-225 stands glass sand with the d_{50} of 225 μm.

and/or SCMs for sustainability purposes, and to promote hydration reactions that further refine the microstructure and improve the compressive strength, as shown in Fig. 33. As elaborated in Section 3.1.3, fillers provide extra nucleation sites for precipitation of cement hydration products and thus promote the hydration reaction. However, when the addition of nanomaterials exceeds a certain amount, the compressive strengths are reduced due to the agglomeration of nanomaterials forming weak zones [235]. Other nanomaterials follow a similar trend, as reported by other researchers [236–238].

As elaborated in Section 3.2.1, applying internal curing effectively promotes cement hydration in UHPC [240]. Meng et al. [128] successfully used porous sand as an internal curing agent to prepare UHPC with reduced autogenous shrinkage and improved compressive strength.

4.3.2. *Densify hydration products*

Hydration products can be densified by applying heat curing or/and promoting pozzolanic reaction to strengthen UHPC matrix and ITZ, thus improving the compressive strength of UHPC. Fig. 34 shows the compressive strength and proportion of different types of C–S–H. As the fraction of ultra-high-density C–S–H increased from 15.4% to 100%, the compressive strength increased from 150 MPa to 180 MPa (by 20%).

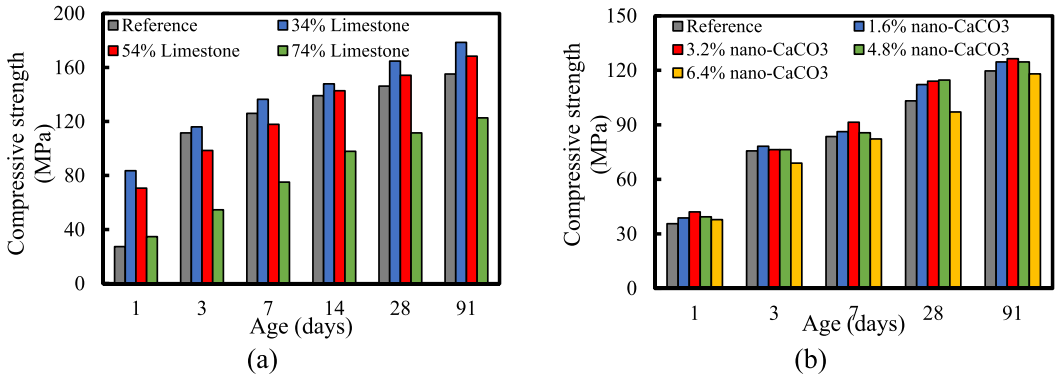

Fig. 33. Results of filler effect on compressive performance of UHPC: (a) micro-scale filler [34]; and (b) nano-scale filler [235,239].

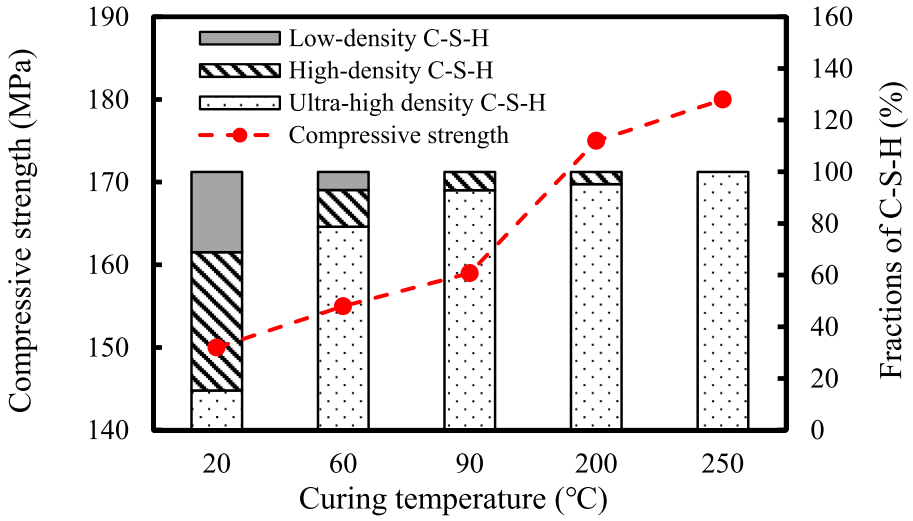

Fig. 34. Results of heat curing on compressive strength and fractions of different types of C–S–H in UHPC [241].

4.4. *Improve flexural/tensile properties*

By using high-volume reinforcing fibers (≥2%, by volume of mixture), UHPC can achieve strain-hardening behavior. However, other than the high cost, a high fiber content can cause handling issues (e.g., hard to mix and low workability due to the fiber agglomeration) [57,242,243]. To minimize the fiber content while retaining or improving flexural/tensile properties, innovative methods have been proposed: (1) improving the fiber dispersion and fiber orientation; and (2) incorporating multi-scale reinforcements.

4.4.1. *Improve fiber dispersion and fiber orientation*

4.4.1.1. Improve fiber dispersion. Fiber dispersion represents the layout of the reinforcing fibers in UHPC and is quantified by the deviation of the number of fibers per unit area from the total number of fibers in the whole cross-section. Fig. 35 shows that uniformly dispersed fibers lead to a higher flexural strength of UHPC beams [244] because an even fiber dispersion can improve the encapsulation effect of the UHPC mortar on the fiber surface and increase the fiber-matrix interfacial properties [245].

Fiber dispersion can be controlled by the viscosity of the UHPC suspending mortar [10]. According to Ref. [206], overall, the coefficient of fiber dispersion (α) increased with the plastic viscosity of UHPC mortar, as shown in Fig. 36(a). Meanwhile, the flexural strength and toughness increased with the coefficient of fiber dispersion, as shown in Fig. 36(b). The slight reduction of flexural strength was due to an increase of entrapped air in the UHPC matrix due to the excessive addition of VMA.

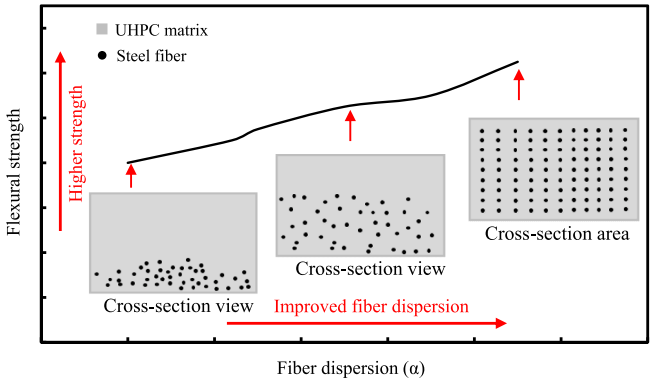

Fig. 35. Relationship between fiber dispersion coefficient and flexural strength of UHPC [246].

4.4.1.2. Improve fiber orientation. The optimal fiber orientation aligns the reinforcing fibers along the direction of tensile stress [247]. For the UHPC cast with the conventional method, the fibers are randomly oriented [248]. According to single-fiber pullout test results, when the

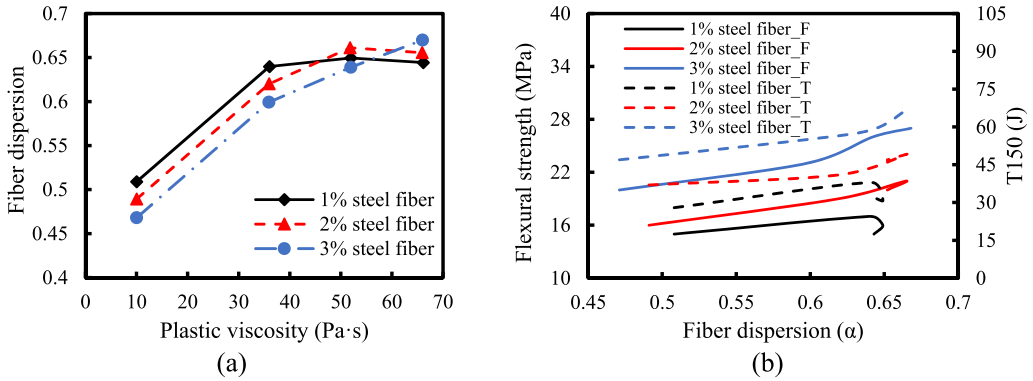

Fig. 36. Results of rheology control for UHPC: (a) the plastic viscosity of UHPC suspension mortar versus fiber dispersion; and (b) fiber dispersion versus the flexural strength of UHPC [206].

angle of reinforcing fibers is over 30° off the tensile direction, the energy dissipation capacity and bond strength can be significantly reduced [249–251]. When more fibers are orientated to the tensile direction, higher flexural properties of UHPC can be achieved, as depicted in Fig. 37 [10].

The casting methods show a significant effect on the fiber orientation [160,252,253]. The best practice for casting a UHPC beam is to induce self-orientation of fibers by allowing the UHPC to flow from one side to the other side of a beam. Due to the high viscosity of UHPC, the velocity gradient of the shear flow of fresh UHPC drives the fibers to be oriented along the flow direction [10]. It is noteworthy that the fiber orientation is dominated by the size of the specimen [253,254]. Huang et al. [254] indicated that the free rotation of fibers was impeded near the formwork boundaries so that the fiber orientation near the formwork is better than that far from the formwork walls (i.e., wall effect), as shown in Fig. 38. The thickness of the wall-effect zone is dependent on the dimension of the molds [254], thinner specimens generally have better fiber orientation when the same casting method is employed.

Besides, Song et al. [253] found the fiber orientation in UHPC was also improved by increasing the length of the casting mold. The casting mold was divided into three zones: (1) adjusting zone: fibers start to re-orient; (2) optimized zone: most of the fibers align to the flow direction; and (3) re-disorder zone: fibers were disordered due to the reduction of flow velocity. As low S_{aver} (the average area of fibers) represents a good fiber orientation (Fig. 39(a)), the S_{aver} value first decreases with the increase of flow distance and increases at the other end of the mold (Fig. 39(b)). When the casting length increased from 400 mm to 1000 mm, the length of the optimized zone was increased from 0 mm to 280 mm (Fig. 39(c)).

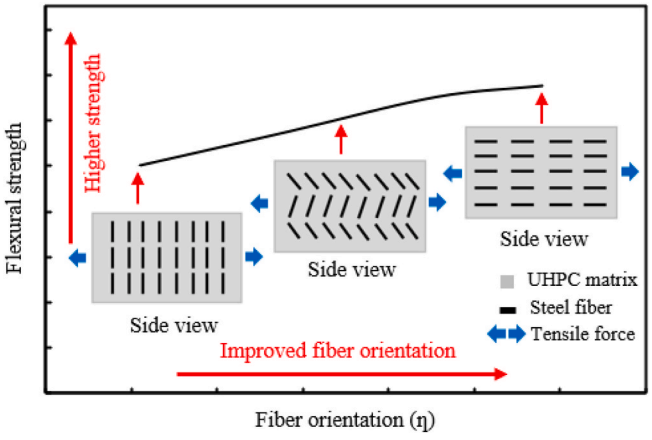

Fig. 37. Relationship between the fiber orientation and the flexural strength of UHPC [246].

4.4.2. *Incorporate multi-scale/physics reinforcements*

4.4.2.1. Use hybrid fibers. The flexural/tensile properties of UHPC are dependent on the material, aspect ratio, shape, and surface condition of fibers. Usually, a single type of fibers are used to prepare UHPC, designated as mono fiber. Recently, multiple types of fibers have been used to improve the flexural/tensile properties of UHPC, designated as hybrid fibers.

(1) Hybrid fibers with different materials

Hybrid fibers with different materials have been proposed to improve multiple properties. For example, basalt fibers have been used to increase the first cracking strength due to their strong chemical bond with cement, although this can hinder the post-cracking behaviors and ductility of UHPC. However, steel has excellent ductility, the hybrid of steel and basalt fibers can result in high first cracking strength as well as good ductility. Kang et al. [42] reported that the first cracking stress of UHPC with 1.0% steel fiber + 0.5% basalt fiber was increased by 40% compared with that of UHPC with 1.5% mono steel fibers [171]. Polyethylene fibers can be incorporated to further improve the ductility [171] because their hydrophobic surfaces can create a porous fiber-matrix interfacial zone and weak bond. Yoo and Kim [171] reported that the strain capacity of UHPC with 1.0% steel fiber + 1.0% PE fiber was increased by 45% compared to that of UHPC with 2% mono steel fiber.

(2) Hybrid fibers with different aspect ratios/scales

Reinforcing fibers with different aspect ratios have been combined to improve the flexural properties of UHPC through multi-scale bridge effects for macro-, meso-, and micro-scale cracks [186,255], as illustrated in Fig. 40. For example, Meng and Khayat first proposed to use graphite nanoplatelets and carbon nanofibers to significantly improve the flexural properties of UHPC [106,174]. The effect of the combination of straight steel fiber with different aspect ratios, e.g., $l_f/d_f = 65$, 97.5, and 100, on the flexural strength was studied, and the results indicated that the combination of 1% long steel fibers ($l_f/d_f = 100$) with 1% medium steel fibers ($l_f/d_f = 97.5$) increased the 28-day flexural strength and deformation by 10% and 25%, respectively, compared with UHPC with 2% mono long steel fibers [256].

(3) Hybrid fibers with different shapes

Reinforcing fibers with different shapes can be combined to improve flexural properties. Deformed fibers can increase the mechanical

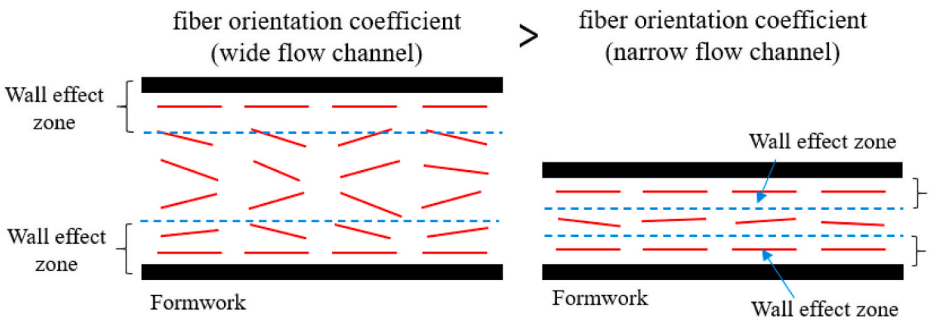

Fig. 38. The illustration of the mechanism of the wall effect [254].

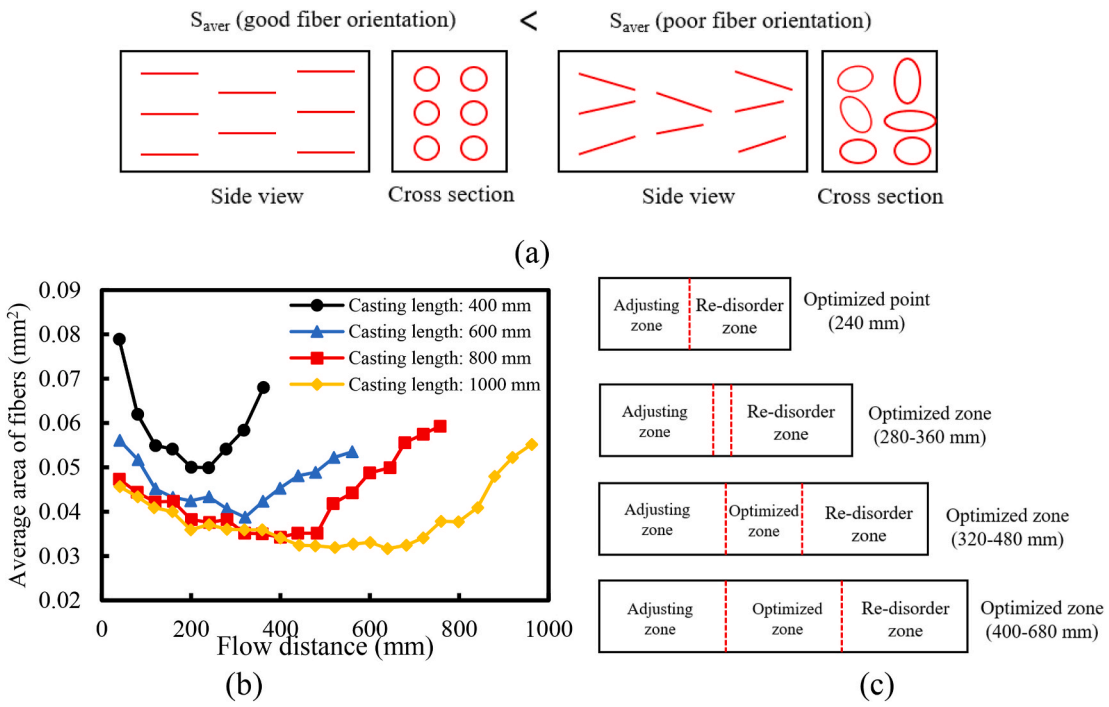

Fig. 39. Fiber orientation in UHPC: (a) effect of fiber orientation on S_{aver}; (b) variation of S_{aver} with flow distance; and (c) the optimized zone in different casting lengths. Note: A low S_{aver} represents a good fiber orientation. The length of the optimized zone increases with the increase of the casting length [253].

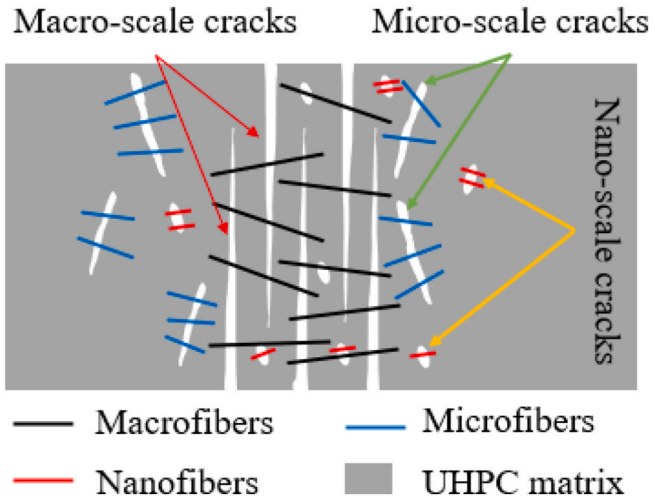

Fig. 40. The mechanism of hybrid fiber reinforcement (with different fiber aspect ratios) on flexural performance of UHPC.

interlock between reinforcing fibers and the UHPC matrix, thus improving the flexural/tensile properties of UHPC, as elucidated in Section 3.4.3 [163]. However, in some cases, the use of high-volume deformed fibers decreases the tensile/flexural properties of UHPC [57, 257]. This is because deformed fibers in the brittle matrix might generate split cracks during the pull-out process, which creates weak zones and deteriorates the reinforced effect of adjacent fiber (Fig. 41). Further, the cost of UHPC using deformed fibers further increases due to the additional manufacturing process of deformed fibers [57]. Therefore, it is recommended to combine deformed fibers with straight fibers. Meng and Khayat [41] found that when the steel fiber content was fixed at 2%, hybrid 1% straight steel fiber with 1% hooked steel fiber achieved the optimal flexural performance. The 28-d flexural strengths were improved by 25% and 30%, and the toughness was increased by 30% and 35%, respectively, compared with that of UHPC with 2% mono straight steel fiber and UHPC with 2% mono hooked steel fiber.

4.4.2.2. Use fiber-reinforced polymer meshes with multi-directional reinforcement. Fiber-reinforced polymer (FRP) meshes can be used to strengthen UHPC elements to achieve high flexural strength and toughness, corrosion resistance, and lightweight property [258,259]. Meng et al. [246,260] studied flexural behaviors of UHPC with steel

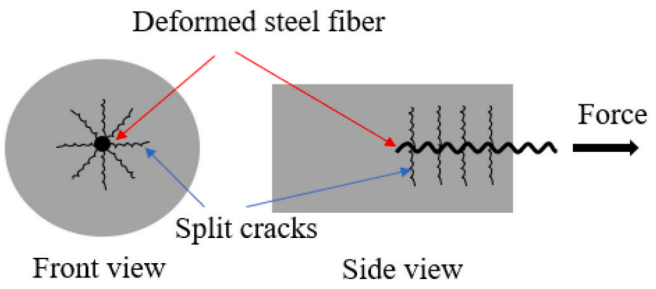

Fig. 41. The use of mono-deformed fiber may cause split cracks and reduce the flexural performance of UHPC [57].

fibers and FRP meshes, including glass FRP (GFRP) and carbon FRP (CFRP, shown in Fig. 42) meshes. The steel fibers restrain the micro-cracks, and the FRP mesh provides two-directional reinforcement to enhance the UHPC panel on a larger scale. The results showed that the combination with 2% steel fiber and a single-layer CFRP increased the peak load and energy dissipation by 35% and 81%, compared with the UHPC panel without FRP [246].

Fig. 43 illustrates a nacre-inspired cementitious-FRP composite structure that was reinforced by polypropylene fibers as well as vinyl-coated polyester FRP [261]. The FRP meshes were placed between the layers of high-strength engineered cementitious composites. This nacre structure can boost the flexural performance of cementitious-FRP composites by isolating the accumulation of damage within each layer, which inherently distributes damage instead of allowing damage to localize at a single weak point to improve the ductility [261–263]. Based on the nacre-inspired composite design schemes, the modulus of rupture, inelastic flexural toughness, and tensile capacity increased by 65%, 520%, and 345%, compared with that of the engineered cementitious composite without FRP meshes [261].

4.5. Improve durability

UHPC exhibits superior durability due to its dense matrix. Table 5 lists the technical specifications, parameters, typical values, and test methods for evaluating the durability of UHPC. The impermeability of UHPC has been proven by the water adsorption and sorptivity tests, which justify the high resistance with the intrusion of detrimental chemical ions (*e.g.*, Cl^- and SO_4^{2-}) and CO_2 [91,264]. However, durability issues exist, which can be attributed to: (1) inappropriate use of porous materials (e.g., SAP and porous sand); (2) crack development under service loads; and (3) alkali-aggregate reaction when recycled materials are used such as recycled concrete aggregate and glass. The solutions for these potential problems are addressed in the following.

4.5.1. Optimize content of porous materials for dense microstructure

As mentioned in Section 4.2, the successful application of porous sand as an internal curing agent in UHPC effectively decreased the autogenous shrinkage of UHPC. Fan et al. [58] studied the effects of porous sand on corrosion of steel reinforcing bars embedded in UHPC and the resistance of the matrix [128]. The results showed that excessive use of porous sand could compromise the corrosion resistance of steel bars and lead to the shortcut of current by the chopped steel fibers in UHPC. This is because, as the porous sand content exceeds the optimum value, the total porosity of UHPC was significantly increased. To mitigate the adverse effect, the replacement ratio of the porous sand should be limited to the optimum value. When below the value, the introduction of pre-saturated porous sand promotes the hydration reaction, and the hydration products fill the pores that help compensate for the porosity introduced by the sand, as shown in Fig. 44. Similarly, the addition of other porous materials in UHPC should be carefully designed and optimized to maintain or improve the microstructure.

4.5.2. Control crack width for corrosion resistance

The superior impermeability of intact UHPC can effectively protect steel reinforcement inside UHPC. However, cracking is inevitable for concrete structures. Cracks provide short paths that facilitate the migration of aggressive ions (e.g., chloride ions and sulfate ions) to contact the steel. Most often, cracks are accompanied by debonding between steel and UHPC, which can damage the passive film on the steel surface and further accelerate corrosion [275]. In this sense, the self-healing of cracks in UHPC is significant for long-term durability. Self-healing of UHPC is attributed to the low degree of cement hydration [276]. Once cracked, unhydrated particles in UHPC are exposed to moisture and air, producing hydration products from hydraulic and/or pozzolanic reactions and precipitating calcium carbonate and C–S–H, as shown in Fig. 45. It is noteworthy that the crack width is critical for self-healing because wide cracks cannot be filled up, and typically it is preferred to control the crack width within 100 μm [277]. The usage of

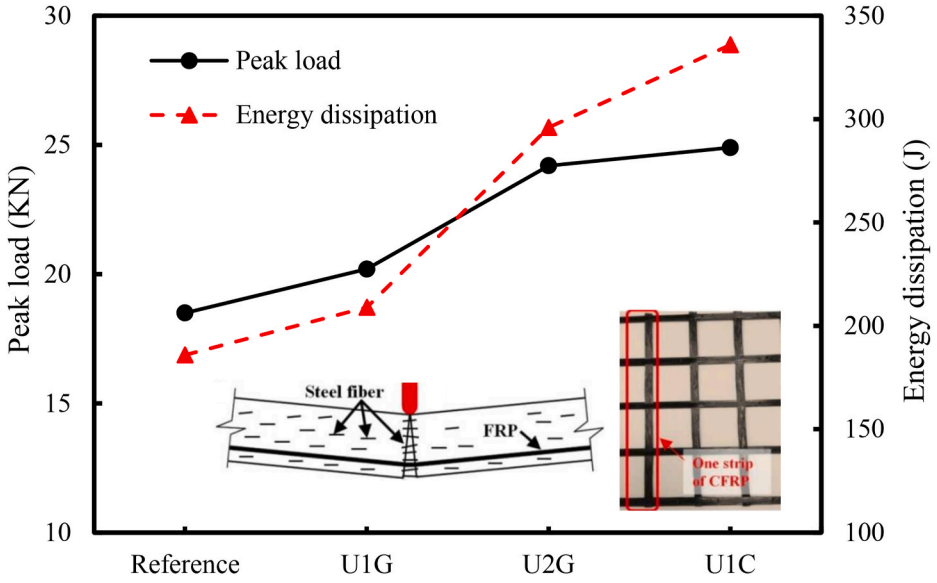

Fig. 42. Flexural behaviors of UHPC with FRP meshes [246]. Reference stands for UHPC without FRP (only 2% steel fiber); U1G stands for 2% steel fiber + single layer GFRP; U2G stands for 2% steel fiber + dual layer GFRP; and U1C-2% steel fiber + single layer CFRP.

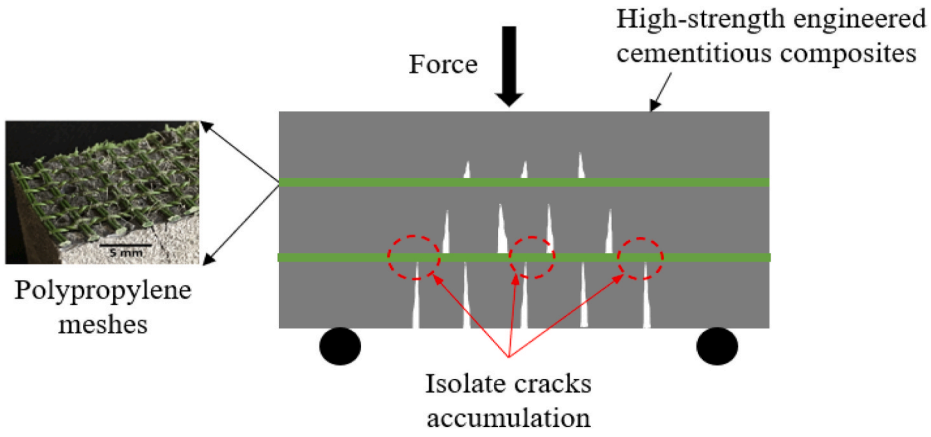

Fig. 43. The mechanism of nacre-inspired cementitious composite structure [261].

Table 5
Test methods, specification, and suggested value of UHPC durability.

Test method	Specification	Parameters	Suggested value	Reference
Water adsorption	ASTM C642	Permeability	<0.005	[265]
Water sorptivity	ASTM C1585	Sorptivity coefficient	<0.044 kg/$m^2/h^{0.5}$	[266, 267]
Alkali-aggregate reaction	ASTM C1567	Expansive percentage	<0.1%	[36,91]
Sulfate resistance	ASTM C1012	Length change	≈0	[268, 269]
Fire resistance	ASTM E119	Residual f_c'	<20%	[170, 270]
Rapid chloride permeability	ASTM C1202	Charge Passed	<100 coulombs	[271, 272]
Freezing-thawing resistance	ASTM C666	Durability factor	>95%	[36,273]
		Mass loss	<0.6%	
Carbonation	ISO 1920–12:2015	Carbonation depth	<3 mm	[268, 274]
Abrasion resistance	ASTM C944	Wearing depth	<1 mm	[36]

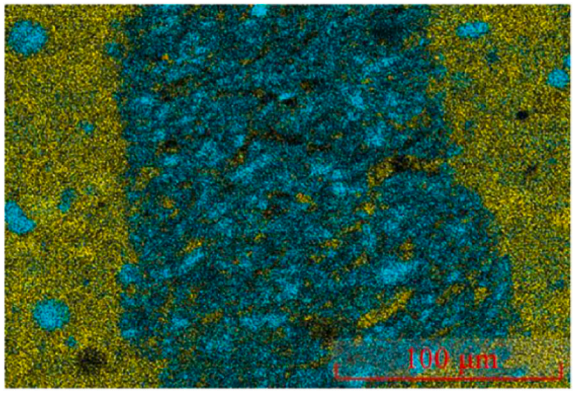

Fig. 44. EDS mapping of interfaces between LWS and matrix [128]. Note: the blue color indicates Si, and the yellow color indicates Ca.

synthetic fibers in UHPC is promising to control crack width. With the introduction of synthetic fibers, the cracking behaviors of UHPC are more prone to multi-micro-cracking patterns rather than localized major cracking patterns. Thus, the number of cracks is increased, and the width of each crack is reduced. In addition, any methods that can reduce autogenous shrinkage and improve the tensile strength of UHPC are promising to improve the crack resistance and control the crack width.

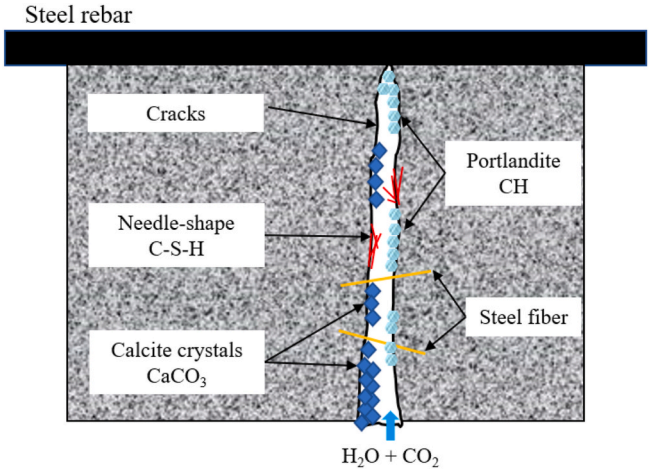

Fig. 45. Schematic illustration of the self-healing phenomenon and the mechanisms in UHPC.

4.5.3. *Limit particle size of reactive materials for ASR resistance*

Reactive aggregates and powders such as waste glass and recycled concrete aggregate have been used to develop cost-effective UHPC mixtures. Under a high pH (>13), the siloxane bond (≡ Si–O–Si ≡) of waste glass is broken, and ≡Si-O^- ions are generated, which can react with alkali ions (K^+, Na^+) to produce ASR gel [105]. An osmotic pressure gradient between the ASR gel and concrete pore solution in concrete drives water and other ions to be absorbed into ASR, which leads to the expansion of ASR gel [278]. As elucidated in Section 3.1, to mitigate the cracking potential of internal ASR, the maximum diameter of the glass powder particles needs to be smaller than the average pore size of UHPC, so the ASR products by glass powder cannot crack the UHPC matrix [279].

5. Representative applications of UHPC

In recent years, UHPC has been attracting increasing interest from the construction industry and it has been applied in numerous structural projects. This section reviews representative structural applications of UHPC.

5.1. *Buildings*

The superior mechanical properties of UHPC enable the design and

fabrication of slender, light, and aesthetically-appealing building components, as shown in Fig. 46. For example, the Museum of European and Mediterranean Civilizations, which is the first building in the world that extensively uses UHPC, was constructed in Marseille, France in 2013. The tree-like façade, brackets and decks of the perimeter footbridges, façade and roof lattices, and the protective covers to the prestressing anchorage points were all made using UHPC [280]. In 2014, Foundation Louis Vuitton pour la Creation was constructed in Paris, France, which features high geometric complexity. The claddings were composed of 19,000 unique and prefabricated UHPC panels [281]. UHPC was also used to construct the roof of the Jean Bouin Stadium in Paris [282], the roof of the Olympic Museum in Lausanne [283], and the cladding for the Qatar National Museum [284]. Besides, a 4-m-high freeform pillar was fabricated using UHPC in Provence, France [285].

5.2. Bridges

Compared with buildings, bridges are generally subjected to higher live loads, so UHPC has been proven a promising material for bridges, as shown in Fig. 47. In 2006, the first UHPC bridge – Mars Hill bridge (Fig. 47(a)) in the United States was built in Wapello County, Iowa, United States. The 33.5-m-long I-shaped prestressed bridge girders were fabricated using UHPC. The superior compressive strength of UHPC helped reduce the amount of prestress tendons and the girder depth [286]. Based on the success of the project, the shape of UHPC girder was further optimized, and Pi-shaped girders were designed, as shown in Fig. 47(b). With the optimized design, the Jakway Park Bridge showed excellent performance after it was open to traffic [287]. The successful development of Pi-shaped UHPC girder greatly expanded the application of UHPC in bridges. However, the high upfront cost of proprietary UHPC used in the two projects prevented wider acceptance of UHPC in other states. Therefore, cost-effective locally-available materials have been utilized to develop non-proprietary cost-effective UHPC. However, the feasibility of using non-proprietary UHPC as structural elements of bridges needs to be further investigated.

In addition to the cast-in-place bridge girders, precast UHPC elements have been widely used in Accelerated Bridge Construction (ABC) projects. In 2011, the first precast UHPC waffle bridge deck panels were installed in the Little Cedar Creek Bridge in Wapello County, Iowa [288], as shown in Fig. 47(c). After bridge construction, no fatigue damage was

Fig. 46. Representative applications of UHPC in buildings: (a) Museum of European and Mediterranean Civilizations [280]; (b) Foundation Louis Vuitton pour la Creation [281]; (c) Jean Bouin Stadium [282]; (d) Olympic Museum in Lausanne [283]; (e) Qatar National Museum [284]; and (f) a 4-m-high pillar fabricated via 3D printing [285].

Fig. 47. Representative applications of UHPC in bridges: (a) I-shaped girder [286]; (b) Pi-shaped girder [287]; (c) precast waffle bridge deck panels [288]; (d) joint connection [289]; (e) bridge deck overlay [291]; and (f) pier jacket [293].

found, and the displacements of the bridge deck were considerably smaller than the allowable limits.

Another application of UHPC is a filed-cast joint connection for bridge decks, which is commonly implemented in the ABC projects. The typical connection requires complicated reinforcement layouts which is time-consuming. The use of UHPC simplifies the on-site assembling process for reinforcement and shortens the construction time [289]. In 2009, two field-cast UHPC connection projects (Route 31 Bridge in Lyons and Route 23 Bridge in Oneonta) were successfully implemented, as shown in Fig. 47(d) [290].

Most currently, in the U.S., UHPC has been applied for the repair and rehabilitation of deteriorated bridge decks and columns/piers. In 2017, the first UHPC bridge deck overlay was constructed in Buchanan County, Iowa States (Mud Creek Bridge) [291], as shown in Fig. 47(e). The field test showed satisfactory bonding properties between the UHPC overlay and substrates, as well as commendable crack resistance of the overlay [292]. However, given the slope of the bridge deck, when applied as an overlay, the UHPC mixtures should be designed with thixotropic property for the slope casting; otherwise, the UHPC mixture would flow freely under gravity due to the slope, and the formworks must be used, which further increases the construction cost. Design a thixotropic UHPC can help mitigating or even eliminating the use of formworks [292]. Further, to improve the seismic behavior, spalling resistance, and corrosion resistance of the concrete bridge pier, the UHPC was also applied as a pier jacket. In 2014, one of the UHPC pier jacket projects was constructed in Canada (The Mission Bridge) [293], as shown in Fig. 47(f).

5.3. Other applications

In addition to buildings and bridges, it is promising to apply UHPC to other structures, such as tunnels, wind turbine towers, and nuclear power plants. For tunnel application, UHPC can develop more efficient tunnel systems with larger useable spaces by reducing the thickness of tunnel elements [294]. For wind turbine towers, UHPC components allow for the creation of taller and more slender wind turbine towers, thus increasing the efficiency of energy generation [295]. For nuclear power plants, UHPC possesses better radiation shielding property and

higher blast tolerance which can better guarantee the security of critical infrastructure [296].

6. Conclusions and further research

6.1. Conclusions

A critical review is carried out on new development of UHPC mixtures. The mixture design methodologies and typical ingredients of UHPC are comprehensively introduced. Besides, as an effort to resolve some challenges associated with the UHPC, some state-of-art solutions are summarized. Finally, some representative applications are introduced. Based on that, the following conclusions can be drawn:

(1) The main mixture design methodologies for UHPC include the dry particle packing method, wet particle packing method, and performance-based method. The principle of the dry particle packing method and wet particle packing method is to maximize the initial packing density of UHPC. The performance-based method is to directly link the design variables with the target properties of UHPC.
(2) The typical ingredients of UHPC include: (1) binder materials: SCMs and fillers (2) aggregates: fine aggregates and coarse aggregates; (3) chemical admixtures; (4) reinforced fibers. The unique properties, recommended contents, effects on UHPC properties, and the working principles of the ingredients have been comprehensively reviewed.
(3) The workability of UHPC should be well controlled for constructability. The physical control and chemical control are elucidated to effectively improve the flowability of UHPC to guarantee the self-consolidating property. The adjustment of viscosity modified agent content is proposed to control the rheology of UHPC suspending mortar to prevent fiber segregation and floating of lightweight raw materials.
(4) Four effective methods to reduce the autogenous shrinkage of UHPC are discussed, including control degree of cement hydration, reduction rate of internal relative humidity, restraint degree for volume change, and introduction of internal forces to compensate shrinkage-induced tension.
(5) Two methods to improve the flexural/tensile properties are summarized, including fiber dispersion and fiber orientation improvement and incorporation of multiscale/physics reinforcements
(6) Three potential durability issues and corresponding solutions are proposed. The content of porous materials needs to be optimized to prevent affecting the porosity of UHPC. The crack width needs to be controlled within 0.1 mm to allow sufficient self-healing. The particle size of reactive aggregates needs to be restricted to prevent ASR cracking.

6.2. Future research trend

Based on the above review, some future research opportunities have been identified as follows:

(1) The unit weight of UHPC is high due to the use of steel components. Future studies should be conducted to further reduce the unit weight of UHPC for lightweight structures and repair and rehabilitation applications.
(2) Some specific nanomaterials can provide UHPC with functionality, such as self-sensing property, self-cleaning property, and electromagnetic interference shielding property. More research can be done in the area.
(3) SCMs such as slag, fly ash, and silica fume are important components in UHPC mixture design. However, due to the switching from coal to natural gas power plants, the typical SCMs are scarcer. As a result, research on alternative SCMs is highly in demand.
(4) UHPC usually contains high volumes of binders which can be used to sequester recycled or atmospheric CO_2 while improving the mechanical properties and durability of the UHPC. The technologies of CO_2 sequestration by the UHPC are of interest to be developed.

Declaration of competing interest

The authors declare that they have no known competing financial interests or personal relationships that could have appeared to influence the work reported in this paper.

Acknowledgements

This paper is supported by National Science Foundation under award: CMMI 2046407 and New Jersey Department of Transportation: Task Order 349 – Bridge Resource Program (2017-2020), contract ID number: 17-60139, federal project number: D00S237. The authors thank Mr. Leo Boyer for editing the language of the manuscript.

Appendix

Table A
Commercial UHPC mixture designs

Designation formulation (kg/m^3)										Mini slump (mm)	28-day f_c' (MPa)	Reference
Code	Premix	Cement	SF	QP	Sand	AC	HRWR	Water	Steel fiber			
Ductal®	–	712	231	211	1020	30	31	109	156	180 ± 20	149	[22,23]
BSI®	–	1114	169	–	1072	–	40	209	234	640*	175	[24]
CEMTEC®	–	1050	268	–	514	–	44	180	470	–	205☆	[25]
CRC®	930	–	–	–	1300	–	–	150	225	–	150	[26]
BCV®	2136	–	–	–	–	–	21.5	–	156	750*	140	[27]
Cor-Tuf®	–	758	497	295	733	–	13	158	140	–	>200⊙	[28]

Note: Premix stands for the combination of all cementitious materials (proportion is unknown), QP stands for quartz powder; AC stands for accelerator; f_c' stands for compressive strength, * stands for slump flow results, ☆ stands for heat curing, ⊙ stands for the special curing method (moisture curing at 22 °C and 100% for 8 days, then cured in water bath at 85 °C for 4 days, finally dried in an oven for 2 days at 85 °C for a cumulative age of 13 days).

Table B1
UHPC mixture designs (using high-volume SCMs)

Designation formulation (kg/m^3)												Mini slump (mm)	28-day $f_c^{'}$ (MPa)	Reference
Code	Cement	SF	QP	FA	Slag	GP	RHA	NP	Sand	HRWR	Water	Steel fiber			
G50SF5	548	42	–	–	535	–	–	–	998	16.0	167	156	280	125	[31]
G50	593	–	–	–	546	–	–	–	993	12.5	182	156	285	124	
FAC40SF5	663	42	–	367	–	–	–	–	1011	12.0	171	156	285	124	
FAC60	486	–	–	556	–	–	–	–	1019	5.5	188	156	285	120	
80C20 GP	623	216	–	–	–	390	–	–	935	13.0	188	158	217	170	[32]
U1-RHA	781	–	208	–	–	–	155	–	1029	23.4	202	78	280	170	[33]
U2-RHA	579	–	208	–	183	–	155	–	1029	22.9	203	78	315	185	
M2	900	110		–	–	–	–	110	1036	40.0	163	157	184	138	[297]
M5	630	220		–	–	–	–	270	994	40.0	163	157	184	131	

Note: SF stands for silica fume, QP stands for quartz powder; FA stand for fly ash, GP stands for glass powder, RHA stands for rice husk ash, NP stands for natural pozzolan, HRWR = high-range water reducer. All UHPC mixtures are under standard curing, $f_c^{'}$ stands for compressive strength.

Table B2
UHPC mixture designs (use high-volume fillers)

Designation formulation (kg/m^3)											Mini slump (mm)	28-day $f_c^{'}$ (MPa)	Reference
Code	Cement	SF	LSP	QP	NS	NC	Sand	HRWR	Water	Steel fiber			
LP25C	595	198	198	278	–	–	873	7.1	191	162	–	160	[35]
LP50C	397	198	397	278	–	–	873	4.7	191	162	–	130	
CSFLS34	826	192	486	–	–	–	444	10.5	201	–	360	148	[34]
NC3.2-2	829	216	–	–	–	34.5	923	NG	177	156	220–250	115	[113]
NS1.0-2	852	216	–	–	10.8	–	923	NG	177	156	220–250	114	
NS1	900	135	–	–	10.4	–	1125	22.5	186	78	–	132	[235]

Note: SF stands for silica fume, LSP stands for limestone powder, QP stands for quartz powder, NS stands for nano-silica, NC stands for nano-$CaCO_3$, $f_c^{'}$ stands for compressive strength.

Table B3
UHPC mixture designs (low powder content by incorporating coarse aggregates)

Designation formulation (kg/m^3)									Mini slump (mm)	28-day $f_c^{'}$ (MPa)	Reference
Code	Cement	SF	LSP	Sand	Coarse aggregates	HRWR	Water	Steel fiber			
UHPC1	675	45	180	864	576 (Max size = 3 mm)	10.8	180	156	–	142	[38]
UHPC2	675	45	180	588	895 (Max size = 8 mm)	10.8	180	156	–	139	
UHPC3	675	45	180	304	1189 (Max size = 16 mm)	10.8	180	156	–	136	
1–1	450	50	–	797	1195 (Max size = 19 mm)	18.0	90	–	200*	131	[39]
1–2	630	70	–	715	1073 (Max size = 19 mm)	18.0	126	–	270*	135	
1–3	810	90	–	616	923 (Max size = 19 mm)	18.0	162	–	550*	138	

Note: SF stands for silica fume, LSP stands for limestone powder, HRWR stands for high-range water reducer, $f_c^{'}$ stands for compressive strength.

Table B4
UHPC mixture designs (hybrid fibers)

Designation formulation							28-day $f_c^{'}$ (MPa)	28-day $f_f^{'}$ (MPa)	28-day $f_t^{'}$ (MPa)	Toughness T150 (J)	Reference
Code	SF	BF	PVA	GF	WF	CF					
MGF 1.5	–	–	–	1%	–	–	152	11.2		–	[166]
S1.0-B0.5	1%	0.5%	–	–	–	–	128	–	14.7	–	[42]
S1.0-PVA0.5	1%	–	0.5%	–	–	–	143	–	11.8	–	[42]
PVA0.5S1.5	1.5%	–	0.5%	–	–	–	160	23.4	–	58.5	[41]
Basalt 1	–	1%	–	–	–	–	139	–	–	–	[169]
Wollastonite	–	–	–	–	1%	–	145	–	–	–	[169]
UHPC-J10	–	–	–	–	–	10*	118	13.8	–	–	[298]

Note: SF stands for steel fiber, BF stands for basalt fiber, PVA stands for polyvinyl alcohol fiber, GF stands for glass fiber, WF stands for wollastonite fiber, CF stands for cellulose fiber, $f_c^{'}$ stands for compressive strength, $f_f^{'}$ stands for flexural strength, * stands for kg/m^3, $f_t^{'}$ stands for tensile strength.

Table C
Proportioning of the Reference UHPC mixture

Designation formulation (kg/m^3)								Mini slump (mm)	28-day $f_c^{'}$ (MPa)	28-day $f_f^{'}$ (MPa)	Toughness T150 (J)	Autogenous shrinkage (μm/m)	Reference
Code	Cement	SF	QS	FS	HRWR	Water	Steel fiber						
Reference	712	231	1020	211	6.5	164	156	275	135	19.7	40.4	730	[31]

Note: Reference UHPC mixture is under standard curing.

References

[1] De la Varga I, Graybeal BA. Dimensional stability of grout-type materials used as connections between prefabricated concrete elements. J Mater Civ Eng 2015;27(9). 04014246.
[2] Wille K, Naaman AE, Parra-Montesinos GJ. Ultra-high performance concrete with compressive strength exceeding 150 MPa (22 ksi): a simpler way. ACI Mater J 2011;108(1).
[3] Habel K, Viviani M, Denarié E, Brühwiler E. Development of the mechanical properties of an ultra-high performance fiber reinforced concrete (UHPFRC). Cement Concr Res 2006;36(7):1362–70.
[4] Meng Q, Wu C, Li J, Liu Z, Wu P, Yang Y, Wang Z. Steel/basalt rebar reinforced Ultra-High Performance Concrete components against methane-air explosion loads. Compos B Eng 2020;198:108215.
[5] Li P, Sluijsmans MJ, Brouwers H, Yu Q. Functionally graded ultra-high performance cementitious composite with enhanced impact properties. Compos B Eng 2020;183:107680.
[6] Perry V. What really is ultra-high performance concrete – towards a global definition. In: Proceedings of the 2nd international conference on UHPC materials and structures. Fuzhou: RILEM Publications; 2018.
[7] Russell HG, Graybeal BA, Russell HG. Ultra-high performance concrete: a state-of-the-art report for the bridge community. United States: Federal Highway Administration. Office of Infrastructure Research and Development; 2013.
[8] ACI 239R-18 ultra-high-performance concrete: an emerging technology report. American Concrete Institute; 2018.
[9] Graybeal BA. Flexural behavior of an ultrahigh-performance concrete I-girder. J Bridge Eng 2008;13(6):602–10.
[10] Meng W, Khayat KH. Improving flexural performance of ultra-high-performance concrete by rheology control of suspending mortar. Compos B Eng 2017;117:26–34.
[11] Vande Voort TL, Suleiman MT, Sritharan S. Design and performance verification of UHPC piles for deep foundations. Iowa State University. Center for Transportation Research and Education; 2008.
[12] Liu, Z. and Meng, W., Fundamental understanding of carbonation curing and durability of carbonation-cured cement-based composites: a review. J. CO2 Util., 44, pp: 101428.
[13] Li Y, Mi T, Liu W, Dong Z, Dong B, Tang L, Xing F. Chemical and mineralogical characteristics of carbonated and uncarbonated cement pastes subjected to high temperatures. Compos B Eng 2021;216:108861.
[14] Azmee NM, Shafiq N. Ultra-high performance concrete: from fundamental to applications. Case Stud. Construct. Mater. 2018;9.
[15] Birchall J, Howard A, Kendall K. Flexural strength and porosity of cements. Nature 1981;289(5796):388–90.
[16] Bache HH. Densified cement ultra-fine particle-based materials. 1981.
[17] Kar DRL. Properties, applications: slurry infiltrated fiber concrete (SIFCON). Concr Int 1984;6(12):44–7.
[18] Bache HH. Compact reinforced composite basic principles. 1987.
[19] Lankard DR. Slurry infiltrated fiber concrete (SIFCON): properties and applications. MRS Online Proc Libr 1984;42.
[20] Richard P, Cheyrezy M. Composition of reactive powder concretes. Cement Concr Res 1995;25(7):1501–11.
[21] De Larrard F, Sedran T. Optimization of ultra-high-performance concrete by the use of a packing model. Cement Concr Res 1994;24(6):997–1009.
[22] Graybeal BA. Compressive behavior of ultra-high-performance fiber-reinforced concrete. ACI Mater J 2007;104(2):146.
[23] Graybeal BA. Material property characterization of ultra-high performance concrete. United States: Federal Highway Administration. Office of Infrastructure Research and Development; 2006.
[24] Hajar Z, Lecointre D, Simon A, Petitjean J. Design and construction of the world first ultra-high performance concrete road bridges. In: Proceedings of the Int. Symp. On UHPC; 2004. Kassel, Germany.
[25] Rossi P, Arca A, Parant E, Fakhri P. Bending and compressive behaviours of a new cement composite. Cement Concr Res 2005;35(1):27–33.
[26] Aarup B. CRC–Structural applications of ultra high performance fiber reinforced concrete. In: Proceedings of the Second international symposium on ultra high performance concrete; March. 2008.
[27] Camacho E, López J, Ros PS. Definition of three levels of performance for UHPFRC-VHPFRC with available materials. In: Ultra-high performance concrete and nanotechnology in construction. Proceedings of hipermat 2012. 3rd international symposium on UHPC and nanotechnology for high performance construction materials. Kassel University Press; 2012.
[28] Williams EM, Graham SS, Reed PA, Rushing TS. Laboratory characterization of Cor-Tuf concrete with and without steel fibers. Enginner research and development center; 2009.
[29] Ahmad S. Use of alternative waste materials in producing ultra-high performance concrete. In: MATEC web of conferences. EDP Sciences; 2017.
[30] Chen Y, Matalkah F, Soroushian P, Weerasiri R, Balachandra A. Optimization of ultra-high performance concrete, quantification of characteristic features. Cogent Eng. 2019;6(1):1558696.
[31] Meng W, Valipour M, Khayat KH. Optimization and performance of cost-effective ultra-high performance concrete. Mater Struct 2017;50(1):29.
[32] Soliman N, Tagnit-Hamou A. Development of ultra-high-performance concrete using glass powder–Towards ecofriendly concrete. Construct Build Mater 2016;125:600–12.
[33] Rößler C, Bui D-D, Ludwig H-M. Rice husk ash as both pozzolanic admixture and internal curing agent in ultra-high performance concrete. Cement Concr Compos 2014;53:270–8.
[34] Huang W, Kazemi-Kamyab H, Sun W, Scrivener K. Effect of cement substitution by limestone on the hydration and microstructural development of ultra-high performance concrete (UHPC). Cement Concr Compos 2017;77:86–101.
[35] Kang S-H, Jeong Y, Tan KH, Moon J. High-volume use of limestone in ultra-high performance fiber-reinforced concrete for reducing cement content and autogenous shrinkage. Construct Build Mater 2019;213:292–305.
[36] Berry M, Snidarich R, Wood C. Development of non-proprietary ultra-high performance concrete. Montana: Dept. of Transportation. Research Programs; 2017.
[37] Subedi D. Non-proprietary UHPC for anchorage of large diameter column bars in grouted ducts. Doctoral dissertation. 2019.
[38] Li P, Yu Q, Brouwers H. Effect of coarse basalt aggregates on the properties of Ultra-high Performance Concrete (UHPC). Construct Build Mater 2018;170:649–59.
[39] Wang C, Yang C, Liu F, Wan C, Pu X. Preparation of ultra-high performance concrete with common technology and materials. Cement Concr Compos 2012;34(4):538–44.
[40] Wu Z, Shi C, Khayat KH. Investigation of mechanical properties and shrinkage of ultra-high performance concrete: influence of steel fiber content and shape. Compos B Eng 2019:107021.
[41] Meng W, Khayat KH. Effect of hybrid fibers on fresh properties, mechanical properties, and autogenous shrinkage of cost-effective UHPC. J Mater Civ Eng 2018;30(4):04018030.
[42] Kang ST, Choi JI, Koh KT, Lee KS, Lee BY. Hybrid effects of steel fiber and microfiber on the tensile behavior of ultra-high performance concrete. Compos Struct 2016;145:37–42.
[43] Zhang H, Ji T, He B, He L. Performance of ultra-high performance concrete (UHPC) with cement partially replaced by ground granite powder (GGP) under different curing conditions. Construct Build Mater 2019;213:469–82.
[44] Zhang H, Ji T, Zeng X, Yang Z, Lin X, Liang Y. Mechanical behavior of ultra-high performance concrete (UHPC) using recycled fine aggregate cured under different conditions and the mechanism based on integrated microstructural parameters. Construct Build Mater 2018;192:489–507.
[45] Schachinger I, Hilbig H, Stengel T, Fehling E. Effect of curing temperature at an early age on the long-term strength development of UHPC. In: 2nd international symposium on ultra high performance concrete. Kassel University Press; 2008.
[46] Yu R, Spiesz P, Brouwers H. Development of an eco-friendly Ultra-High Performance Concrete (UHPC) with efficient cement and mineral admixtures uses. Cement Concr Compos 2015;55:383–94.
[47] El-Tawil S, Tai Y-S, Meng B, Hansen W, Liu Z. Commercial production of non-proprietary ultra high performance concrete. Michigan Department of Transportation Research Administration; 2018.
[48] Ramme BW, Tharaniyil MP. Coal combustion products utilization handbook. 2004.
[49] Qiao P, Zhou Z, Allena S. Developing connections for longitudinal joints between deck bulb tees-development of UHPC mixes with local materials. Washington (State): Department of Transportation; 2016.
[50] Berry M, Scherr R, Matteson K. Feasibility of non-proprietary ultra-high performance concrete (UHPC) for use in highway bridges in Montana: phase II field application. Montana Department of Transportation; 2020.
[51] Mendonca F, El-Khier MA, Morcous G, Hu J. Feasibility study of development of ultra-high performance concrete (UHPC) for highway bridge applications in Nebraska. Nebraska Department of Transportation; 2020.
[52] Yoo D-Y, Park J-J, Kim S-W, Yoon Y-S. Influence of reinforcing bar type on autogenous shrinkage stress and bond behavior of ultra high performance fiber reinforced concrete. Cement Concr Compos 2014;48:150–61.
[53] Valipour M, Khayat KH. Coupled effect of shrinkage-mitigating admixtures and saturated lightweight sand on shrinkage of UHPC for overlay applications. Construct Build Mater 2018;184:320–9.
[54] Cusson D, Hoogeveen T. An experimental approach for the analysis of early-age behaviour of high-performance concrete structures under restrained shrinkage. Cement Concr Res 2007;37(2):200–9.
[55] Teng L, Valipour M, Khayat KH. Design and performance of low shrinkage UHPC for thin bonded bridge deck overlay. Cement Concr Compos 2021:103953.
[56] Zhu L, Wang J-J, Li X, Zhao G-Y, Huo X-J. Experimental and numerical study on creep and shrinkage effects of ultra high-performance concrete beam. Compos B Eng 2020;184:107713.
[57] Yoo D-Y, Kim S, Park G-J, Park J-J, Kim S-W. Effects of fiber shape, aspect ratio, and volume fraction on flexural behavior of ultra-high-performance fiber-reinforced cement composites. Compos Struct 2017;174:375–88.
[58] Fan L, Meng W, Teng L, Khayat KH. Effects of lightweight sand and steel fiber contents on the corrosion performance of steel rebar embedded in UHPC. Construct Build Mater 2020;238:117709.
[59] Yu R, Spiesz P, Brouwers H. Mix design and properties assessment of ultra-high performance fibre reinforced concrete (UHPFRC). Cement Concr Res 2014;56:29–39.
[60] Li L, Kwan A. Packing density of concrete mix under dry and wet conditions. Powder Technol 2014;253:514–21.
[61] Wong HH, Kwan AK. Packing density of cementitious materials: part 1—measurement using a wet packing method. Mater Struct 2008;41(4):689–701.
[62] Stovall T, De Larrard F, Buil M. Linear packing density model of grain mixtures. Powder Technol 1986;48(1):1–12.

[63] De Larrard F, Sedran T. Mixture-proportioning of high-performance concrete. Cement Concr Res 2002;32(11):1699–704.
[64] Fennis S, Walraven J, Den Uijl J. Compaction-interaction packing model: regarding the effect of fillers in concrete mixture design. Mater Struct 2013;46(3):463–78.
[65] Fuller WB, Thompson SE. The laws of proportioning concrete. 1907.
[66] Andreasen A. Über die Beziehung zwischen Kornabstufung und Zwischenraum in Produkten aus losen Körnern (mit einigen Experimenten). Kolloid Z 1930;50(3):217–28.
[67] Funk JE, Dinger DR. Predictive process control of crowded particulate suspensions: applied to ceramic manufacturing. Springer Science & Business Media; 2013.
[68] De Larrard F. Concrete mixture proportioning: a scientific approach. CRC Press; 1999.
[69] Brouwers H, Radix H. Self-compacting concrete: theoretical and experimental study. Cement Concr Res 2005;35(11):2116–36.
[70] Hunger M. An integral design concept for ecological self-compacting concrete. 2010.
[71] Mehdipour I, Khayat KH. Understanding the role of particle packing characteristics in rheo-physical properties of cementitious suspensions: a literature review. Construct Build Mater 2018;161:340–53.
[72] Wang X, Yu R, Song Q, Shui Z, Liu Z, Wu S, Hou D. Optimized design of ultra-high performance concrete (UHPC) with a high wet packing density. Cement Concr Res 2019;126:105921.
[73] Iveson SM, Litster JD, Hapgood K, Ennis BJ. Nucleation, growth and breakage phenomena in agitated wet granulation processes: a review. Powder Technol 2001;117(1–2):3–39.
[74] Iveson SM, Wauters PA, Forrest S, Litster JD, Meesters GM, Scarlett B. Growth regime map for liquid-bound granules: further development and experimental validation. Powder Technol 2001;117(1–2):83–97.
[75] Cai W. Effect of particle packing on flow property and strength of concrete mortar. 2017.
[76] Li L, Cai Z, Yu K, Zhang YX, Ding Y. Performance-based design of all-grade strain hardening cementitious composites with compressive strengths from 40 MPa to 120 MPa. Cement Concr Compos 2019;97:202–17.
[77] ASTM C150/C150M-20. Standard specification for portland cement. ASTM International; 2020.
[78] Taylor HF. Cement chemistry, vol. 2. Thomas Telford London; 1997.
[79] Van, V. and Ludwig, H. Proportioning optimization of UHPC containing rice husk ash and ground granulated blast-furnace slag. in Proceedings of the 3rd international symposium on UHPC and nanotechnology for high performance construction materials, Kassel University Press.
[80] Schröfl C, Gruber M, Plank J. Preferential adsorption of polycarboxylate superplasticizers on cement and silica fume in ultra-high performance concrete (UHPC). Cement Concr Res 2012;42(11):1401–8.
[81] Liao W, Sun X, Kumar A, Sun H, Ma H. Hydration of binary portland cement blends containing silica fume: a decoupling method to estimate degrees of hydration and pozzolanic reaction. Front. Mater. 2019;6:78.
[82] Yu R, Spiesz P, Brouwers H. Effect of nano-silica on the hydration and microstructure development of Ultra-High Performance Concrete (UHPC) with a low binder amount. Construct Build Mater 2014;65:140–50.
[83] Wu Z, Shi C, Khayat K. Influence of silica fume content on microstructure development and bond to steel fiber in ultra-high strength cement-based materials (UHSC). Cement Concr Compos 2016;71:97–109.
[84] Qasim OA. Experimental investigation on autogenous shrinkage of high and ultra-high strength concrete. IOP Conf Ser Mater Sci Eng 2018;454:012067.
[85] Van V-T-A, Rößler C, Bui D-D, Ludwig H-M. Mesoporous structure and pozzolanic reactivity of rice husk ash in cementitious system. Construct Build Mater 2013;43:208–16.
[86] Huang H, Gao X, Wang H, Ye H. Influence of rice husk ash on strength and permeability of ultra-high performance concrete. Construct Build Mater 2017;149:621–8.
[87] Alsalman A, Dang CN, Martí-Vargas JR, Micah Hale W. Mixture-proportioning of economical UHPC mixtures. J. Build. Eng. 2020;27:100970.
[88] Staquet S, Espion B. Early age autogenous shrinkage of UHPC incorporating very fine fly ash or metakaolin in replacement of silica fume. In: International symposium on ultra high performance concrete. Kessel Germany; 2004.
[89] Liu J, Ou Z, Mo J, Wang Y, Wu H. The effect of SCMs and SAP on the autogenous shrinkage and hydration process of RPC. Construct Build Mater 2017;155:239–49.
[90] Randl N, Steiner T, Ofner S, Baumgartner E, Mészöly T. Development of UHPC mixtures from an ecological point of view. Construct Build Mater 2014;67:373–8.
[91] Soliman NA, Tagnit-Hamou A. Using glass sand as an alternative for quartz sand in UHPC. Construct Build Mater 2017;145:243–52.
[92] Soliman N, Tagnit-Hamou A. Partial substitution of silica fume with fine glass powder in UHPC: filling the micro gap. Construct Build Mater 2017;139:374–83.
[93] Van Tuan N, Ye G, Van Breugel K, Copuroglu O. Hydration and microstructure of ultra high performance concrete incorporating rice husk ash. Cement Concr Res 2011;41(11):1104–11.
[94] ASTM C618-19. Standard specification for coal fly ash and raw or calcined natural pozzolan for use in concrete. ASTM International; 2019.
[95] Yu J, Li G, Leung CKY. Hydration and physical characteristics of ultrahigh-volume fly ash-cement systems with low water/binder ratio. Construct Build Mater 2018;161:509–18.
[96] Zhao S, Sun W. Effect of silica fume and fly ash on pore structures of blended pastes at low water to binder ratios. Adv Cement Res 2015;27(9):506–14.
[97] Wei F, Grutzeck MW, Roy DM. The retarding effects of fly ash upon the hydration of cement pastes: the first 24 hours. Cement Concr Res 1985;15(1):174–84.
[98] Moradian M, Hu Q, Aboustait M, Robertson B, Ley MT, Hanan JC, Xiao X. Direct in-situ observation of early age void evolution in sustainable cement paste containing fly ash or limestone. Compos B Eng 2019;175:107099.
[99] Edwin RS, De Schepper M, Gruyaert E, De Belie N. Effect of secondary copper slag as cementitious material in ultra-high performance mortar. Construct Build Mater 2016;119:31–44.
[100] Chen P, Ma B, Tan H, Liu X, Zhang T, Li C, Yang Q, Luo Z. Utilization of barium slag to improve chloride-binding ability of cement-based material. J Clean Prod 2021;283:124612.
[101] Edwin RS, Gruyaert E, De Belie N. Influence of intensive vacuum mixing and heat treatment on compressive strength and microstructure of reactive powder concrete incorporating secondary copper slag as supplementary cementitious material. Construct Build Mater 2017;155:400–12.
[102] Taha B, Nounu G. Utilizing waste recycled glass as sand/cement replacement in concrete. J Mater Civ Eng 2009;21(12):709–21.
[103] Vaitkevičius V, Šerelis E, Hilbig H. The effect of glass powder on the microstructure of ultra high performance concrete. Construct Build Mater 2014;68:102–9.
[104] Pacheco-Torgal F, Labrincha J, Leonelli C, Palomo A, Chindaprasit P. Handbook of alkali-activated cements, mortars and concretes. Elsevier; 2014.
[105] Guo P, Bao Y, Meng W. Review of using glass in high-performance fiber-reinforced cementitious composites. Cement Concr Compos 2021:104032.
[106] Korpa A, Kowald T, Trettin R. Phase development in normal and ultra high performance cementitious systems by quantitative X-ray analysis and thermoanalytical methods. Cement Concr Res 2009;39(2):69–76.
[107] Fehling E, Schmidt M, Walraven J, Leutbecher T, Frönlich S. Ultra-high performance concrete UHPC: fundamentals. *Design, examples*. Beton-Kalender; 2013.
[108] Poppe A-M, De Schutter G. Cement hydration in the presence of high filler contents. Cement Concr Res 2005;35(12):2290–9.
[109] Zanni H, Cheyrezy M, Maret V, Philippot S, Nieto P. Investigation of hydration and pozzolanic reaction in reactive powder concrete (RPC) using 29Si NMR. Cement Concr Res 1996;26(1):93–100.
[110] De Rosa C. International Programme on Chemical safety (IPCS), concise international chemical assessment document, 61 (CICAD), hydrogen cyanide and cyanides: human health aspects. Indian J Med Res 2005;122(2):180.
[111] Li C. Mechanical and transport properties of recycled aggregate concrete modified with limestone powder. Compos B Eng 2020;197:108189.
[112] Burroughs JF, Shannon J, Rushing TS, Yi K, Gutierrez QB, Harrelson DW. Potential of finely ground limestone powder to benefit ultra-high performance concrete mixtures. Construct Build Mater 2017;141:335–42.
[113] Wu Z, Shi C, Khayat KH, Xie L. Effect of SCM and nano-particles on static and dynamic mechanical properties of UHPC. Construct Build Mater 2018;182:118–25.
[114] Shi C, Wu Z, Xiao J, Wang D, Huang Z, Fang Z. A review on ultra high performance concrete: Part I. Raw materials and mixture design. Construct Build Mater 2015;101:741–51.
[115] Su Y, Li J, Wu C, Wu P, Li Z-X. Influences of nano-particles on dynamic strength of ultra-high performance concrete. Compos B Eng 2016;91:595–609.
[116] Teng L, Zhu J, Khayat KH, Liu J. Effect of welan gum and nanoclay on thixotropy of UHPC. Cement Concr Res 2020;138:106238.
[117] Qian Y. Characterization of structural rebuilding and shear migration in cementitious materials in consideration of thixotropy. Doctoral dissertation. 2017.
[118] Gosens I, Post JA, de la Fonteyne LJ, Jansen EH, Geus JW, Cassee FR, de Jong WH. Impact of agglomeration state of nano-and submicron sized gold particles on pulmonary inflammation. Part Fibre Toxicol 2010;7(1):1–11.
[119] Wu Z, Khayat KH, Shi C, Tutikian BF, Chen Q. Mechanisms underlying the strength enhancement of UHPC modified with nano-SiO2 and nano-CaCO3. Cement Concr Compos 2021;119:103992.
[120] Konsta-Gdoutos MS, Metaxa ZS, Shah SP. Highly dispersed carbon nanotube reinforced cement based materials. Cement Concr Res 2010;40(7):1052–9.
[121] Peyvandi A, Soroushian P, Abdol N, Balachandra AM. Surface-modified graphite nanomaterials for improved reinforcement efficiency in cementitious paste. Carbon 2013;63:175–86.
[122] Ma S, Qian Y, Kawashima S. Experimental and modeling study on the non-linear structural build-up of fresh cement pastes incorporating viscosity modifying admixtures. Cement Concr Res 2018;108:1–9.
[123] Hamed N, El-Feky M, Kohail M, Nasr E-SA. Effect of nano-clay de-agglomeration on mechanical properties of concrete. Construct Build Mater 2019;205:245–56.
[124] Kang S-H, Jeong Y, Tan KH, Moon J. The use of limestone to replace physical filler of quartz powder in UHPFRC. Cement Concr Compos 2018;94:238–47.
[125] Tasong WA, Lynsdale CJ, Cripps JC. Aggregate-cement paste interface: Part I. Influence of aggregate geochemistry. Cement Concr Res 1999;29(7):1019–25.
[126] Liu K, Yu R, Shui Z, Li X, Ling X, He W, Yi S, Wu S. Effects of pumice-based porous material on hydration characteristics and persistent shrinkage of ultra-high performance concrete (UHPC). Materials 2019;12(1):11.
[127] Liu K, Yu R, Shui Z, Li X, Guo C, Yu B, Wu S. Optimization of autogenous shrinkage and microstructure for Ultra-High Performance Concrete (UHPC) based on appropriate application of porous pumice. Construct Build Mater 2019;214:369–81.
[128] Meng W, Khayat KH. Effects of saturated lightweight sand content on key characteristics of ultra-high-performance concrete. Cement Concr Res 2017;101:46–54.

[129] Yang S, Millard S, Soutsos M, Barnett S, Le TT. Influence of aggregate and curing regime on the mechanical properties of ultra-high performance fibre reinforced concrete (UHPFRC). Construct Build Mater 2009;23(6):2291–8.
[130] Bentz DP, Ferraris CF, Jones SZ, Lootens D, Zunino F. Limestone and silica powder replacements for cement: early-age performance. Cement Concr Compos 2017;78:43–56.
[131] Fanghui H, Qiang W, Mutian L, Yingjun M. Early hydration properties of composite binder containing limestone powder with different finenesses. J Therm Anal Calorim 2016;123(2):1141–51.
[132] Scrivener K, Martirena F, Bishnoi S, Maity S. Calcined clay limestone cements (LC3). Cement Concr Res 2018;114:49–56.
[133] Yang R, Yu R, Shui Z, Gao X, Xiao X, Fan D, Chen Z, Cai J, Li X, He Y. Feasibility analysis of treating recycled rock dust as an environmentally friendly alternative material in Ultra-High Performance Concrete (UHPC). J Clean Prod 2020;258:120673.
[134] Liao W, Kumar A, Khayat K, Ma H. Multifunctional lightweight aggregate containing phase change material and water for damage mitigation of concrete. 2019.
[135] Bentur A, Igarashi S-i, Kovler K. Prevention of autogenous shrinkage in high-strength concrete by internal curing using wet lightweight aggregates. Cement Concr Res 2001;31(11):1587–91.
[136] Hwang S-D, Khayat KH, Youssef D. Effect of moist curing and use of lightweight sand on characteristics of high-performance concrete. Mater Struct 2013;46(1):35–46.
[137] Liu J, Han F, Cui G, Zhang Q, Lv J, Zhang L, Yang Z. Combined effect of coarse aggregate and fiber on tensile behavior of ultra-high performance concrete. Construct Build Mater 2016;121:310–8.
[138] Liao K-Y, Chang P-K, Peng Y-N, Yang C-C. A study on characteristics of interfacial transition zone in concrete. Cement Concr Res 2004;34(6):977–89.
[139] Ma J, Orgass M, Dehn F, Schmidt D, Tue N. Comparative investigations on ultra-high performance concrete with and without coarse aggregates. In: International symposium on ultra high performance concrete. Germany: Kassel; 2004.
[140] Peng Y, Wu H, Fang Q, Liu J, Gong Z. Impact resistance of basalt aggregated UHP-SFRC/fabric composite panel against small caliber arm. Int J Impact Eng 2016;88:201–13.
[141] Fládr J, Bílý P. Specimen size effect on compressive and flexural strength of high-strength fibre-reinforced concrete containing coarse aggregate. Compos B Eng 2018;138:77–86.
[142] Senft S, Gallegos S, Manson DP, Gonzales C. Chemical admixtures for concrete. CRC Press; 1999.
[143] Zhang L, Du W, Wang D, Wang F, Fang K, Yu J, Sheng B. Syntheses of polycarboxylate superplasticizers: microwave induction versus conventional thermal induction. Compos B Eng 2021;207:108560.
[144] Ilg M, Plank J. Non-adsorbing small molecules as auxiliary dispersants for polycarboxylate superplasticizers. Colloid Surface Physicochem Eng Aspect 2020;587:124307.
[145] Li P, Yu Q, Brouwers H. Effect of PCE-type superplasticizer on early-age behaviour of ultra-high performance concrete (UHPC). Construct Build Mater 2017;153:740–50.
[146] Roussel N. Understanding the rheology of concrete. Elsevier; 2011.
[147] Van Der Vurst F, Grünewald S, Feys D, Lesage K, Vandewalle L, Vantomme J, De Schutter G. Effect of the mix design on the robustness of fresh self-compacting concrete. Cement Concr Compos 2017;82:190–201.
[148] ZANA R. Introduction to surfactants and surfactant self-assemblies. In: Dynamics of surfactant self-assemblies. CRC Press; 2005. p. 18–52.
[149] Bischoff DL, Toepel A. Laboratory testing of portland cement concrete patch material modified to reduce or eliminate shrinkage. Wisconsin Department of Transportation, Division of Transportation; 2004.
[150] Zhan PM, He ZH. Application of shrinkage reducing admixture in concrete: a review. Construct Build Mater 2019;201:676–90.
[151] Bentz D, Geiker MR, Hansen KK. Shrinkage-reducing admixtures and early-age desiccation in cement pastes and mortars. Cement Concr Res 2001;31(7):1075–85.
[152] Carballosa P, Calvo JG, Revuelta D. Influence of expansive calcium sulfoaluminate agent dosage on properties and microstructure of expansive self-compacting concretes. Cement Concr Compos 2020;107:103464.
[153] Corinaldesi V, Nardinocchi A. Mechanical characterization of Engineered Cement-based Composites prepared with hybrid fibres and expansive agent. Compos B Eng 2016;98:389–96.
[154] Mo L, Deng M, Tang M. Effects of calcination condition on expansion property of MgO-type expansive agent used in cement-based materials. Cement Concr Res 2010;40(3):437–46.
[155] Yoo D-Y, Park J-J, Kim S-W, Yoon Y-S. Combined effect of expansive and shrinkage-reducing admixtures on the properties of ultra high performance fiber-reinforced concrete. J Compos Mater 2014;48(16):1981–91.
[156] Yang L, Shi C, Wu Z. Mitigation techniques for autogenous shrinkage of ultra-high-performance concrete–A review. Compos B Eng 2019;178:107456.
[157] Yan P, Qin X. The effect of expansive agent and possibility of delayed ettringite formation in shrinkage-compensating massive concrete. Cement Concr Res 2001;31(2):335–7.
[158] Higuchi T, Eguchi M, Morioka M, Sakai E. Hydration and properties of expansive additive treated high temperature carbonation. Cement Concr Res 2014;64:11–6.
[159] Liu F, Shen S-L, Hou D-W, Arulrajah A, Horpibulsuk S. Enhancing behavior of large volume underground concrete structure using expansive agents. Construct Build Mater 2016;114:49–55.
[160] Zhang Y, Zhu Y, Qu S, Kumar A, Shao X. Improvement of flexural and tensile strength of layered-casting UHPC with aligned steel fibers. Construct Build Mater 2020;251:118893.
[161] Hung C-C, Lee H-S, Chan SN. Tension-stiffening effect in steel-reinforced UHPC composites: constitutive model and effects of steel fibers, loading patterns, and rebar sizes. Compos B Eng 2019;158:269–78.
[162] Xue G, Yilmaz E, Song W, Cao S. Mechanical, flexural and microstructural properties of cement-tailings matrix composites: effects of fiber type and dosage. Compos B Eng 2019;172:131–42.
[163] Wu Z, Shi C, He W, Wu L. Effects of steel fiber content and shape on mechanical properties of ultra high performance concrete. Construct Build Mater 2016;103:8–14.
[164] Wu Z, Shi C, Khayat KH. Investigation of mechanical properties and shrinkage of ultra-high performance concrete: influence of steel fiber content and shape. Compos B Eng 2019;174:107021.
[165] You I, Yoo D-Y, Kim S, Kim M-J, Zi G. Electrical and self-sensing properties of ultra-high-performance fiber-reinforced concrete with carbon nanotubes. Sensors 2017;17(11):2481.
[166] Gesoglu M, Güneyisi E, Muhyaddin GF, Asaad DS. Strain hardening ultra-high performance fiber reinforced cementitious composites: effect of fiber type and concentration. Compos B Eng 2016;103:74–83.
[167] Yan L, Kasal B, Huang L. A review of recent research on the use of cellulosic fibres, their fibre fabric reinforced cementitious, geo-polymer and polymer composites in civil engineering. Compos B Eng 2016;92:94–132.
[168] Ma R, Guo L, Ye S, Sun W, Liu J. Influence of hybrid fiber reinforcement on mechanical properties and autogenous shrinkage of an ecological UHPFRCC. J Mater Civ Eng 2019;31(5):04019032.
[169] Hannawi K, Bian H, Prince-Agbodjan W, Raghavan B. Effect of different types of fibers on the microstructure and the mechanical behavior of ultra-high performance fiber-reinforced concretes. Compos B Eng 2016;86:214–20.
[170] Liang X, Wu C, Su Y, Chen Z, Li Z. Development of ultra-high performance concrete with high fire resistance. Construct Build Mater 2018;179:400–12.
[171] Yoo D-Y, Kim M-J. High energy absorbent ultra-high-performance concrete with hybrid steel and polyethylene fibers. Construct Build Mater 2019;209:354–63.
[172] Fan L, Meng W, Teng L, Khayat KH. Effect of steel fibers with galvanized coatings on corrosion of steel bars embedded in UHPC. Compos B Eng 2019;177:107445.
[173] Banthia N, Foy C. Marine curing of steel fiber composites. J Mater Civ Eng 1989;1(2):86–96.
[174] Shah SP, Daniel JI, Ahmad SH, Arockiasamy M, Balaguru P, Ball CG, Ball Jr HP, Banthia N, Batson GB, Bentur A. Guide for specifying, proportioning, mixing, placing, and finishing steel fiber reinforced concrete. ACI Mater J 1993;90(1):94–101.
[175] Zhou Y, Xi B, Yu K, Sui L, Xing F. Mechanical properties of hybrid ultra-high performance engineered cementitous composites incorporating steel and polyethylene fibers. Materials 2018;11(8):1448.
[176] Kang S-T, Choi J-I, Koh K-T, Lee KS, Lee BY. Hybrid effects of steel fiber and microfiber on the tensile behavior of ultra-high performance concrete. Compos Struct 2016;145:37–42.
[177] Choi J-I, Lee BY. Bonding properties of basalt fiber and strength reduction according to fiber orientation. Materials 2015;8(10):6719–27.
[178] Ahmad S, Rasul M, Adekunle SK, Al-Dulaijan SU, Maslehuddin M, Ali SI. Mechanical properties of steel fiber-reinforced UHPC mixtures exposed to elevated temperature: effects of exposure duration and fiber content. Compos B Eng 2019;168:291–301.
[179] Huang H, Wang R, Gao X. Improvement effect of fiber alignment on resistance to elevated temperature of ultra-high performance concrete. Compos B Eng 2019;177:107454.
[180] Kim MK, Kim DJ, An Y-K. Electro-mechanical self-sensing response of ultra-high-performance fiber-reinforced concrete in tension. Compos B Eng 2018;134:254–64.
[181] Zhang Y, Ju JW, Chen Q, Yan Z, Zhu H, Jiang Z. Characterizing and analyzing the residual interfacial behavior of steel fibers embedded into cement-based matrices after exposure to high temperatures. Compos B Eng 2020;191:107933.
[182] Akbar A, Liew K. Influence of elevated temperature on the microstructure and mechanical performance of cement composites reinforced with recycled carbon fibers. Compos B Eng 2020;198:108245.
[183] Liu K, Cheng X, Li J, Gao X, Cao Y, Guo X, Zhuang J, Zhang C. Effects of microstructure and pore water on electrical conductivity of cement slurry during early hydration. Compos B Eng 2019;177:107435.
[184] Lee SH, Kim S, Yoo D-Y. Hybrid effects of steel fiber and carbon nanotube on self-sensing capability of ultra-high-performance concrete. Construct Build Mater 2018;185:530–44.
[185] Ozawa M, Parajuli SS, Uchida Y, Zhou B. Preventive effects of polypropylene and jute fibers on spalling of UHPC at high temperatures in combination with waste porous ceramic fine aggregate as an internal curing material. Construct Build Mater 2019;206:219–25.
[186] Chun B, Yoo D-Y. Hybrid effect of macro and micro steel fibers on the pullout and tensile behaviors of ultra-high-performance concrete. Compos B Eng 2019;162:344–60.
[187] Yoo D-Y, Banthia N, Kang S-T, Yoon Y-S. Size effect in ultra-high-performance concrete beams. Eng Fract Mech 2016;157:86–106.
[188] Yoo D-Y, Yoon Y-S. Structural performance of ultra-high-performance concrete beams with different steel fibers. Eng Struct 2015;102:409–23.
[189] Wille K, Kim DJ, Naaman AE. Strain-hardening UHP-FRC with low fiber contents. Mater Struct 2011;44(3):583–98.

[190] Yoo D-Y, Kim J-J, Chun B. Dynamic pullout behavior of half-hooked and twisted steel fibers in ultra-high-performance concrete containing expansive agents. Compos B Eng 2019;167:517–32.
[191] Wu Z, Khayat KH, Shi C. How do fiber shape and matrix composition affect fiber pullout behavior and flexural properties of UHPC? Cement Concr Compos 2018; 90:193–201.
[192] Pompo A, Stupak P, Nicolais L, Marchese B. Analysis of steel fibre pull-out from a cement matrix using video photography. Cement Concr Compos 1996;18(1):3–8.
[193] Laranjeira F, Molins C, Aguado A. Predicting the pullout response of inclined hooked steel fibers. Cement Concr Res 2010;40(10):1471–87.
[194] Yoo DY, Jang YS, Chun B, Kim S. Chelate effect on fiber surface morphology and its benefits on pullout and tensile behaviors of ultra-high-performance concrete. Cement Concr Compos 2021;115:103864.
[195] Oh T, You I, Banthia N, Yoo D-Y. Deposition of nanosilica particles on fiber surface for improving interfacial bond and tensile performances of ultra-high-performance fiber-reinforced concrete. Compos B Eng 2021:109030.
[196] Pi Z, Xiao H, Liu R, Liu M, Li H. Effects of brass coating and nano-SiO2 coating on steel fiber–matrix interfacial properties of cement-based composite. Compos B Eng 2020;189:107904.
[197] Pi Z, Xiao H, Liu R, Li H. Combination usage of nano-SiO2-coated steel fiber and silica fume and its improvement effect on SFRCC. Compos B Eng 2021:109022.
[198] Zhang W, Zou X, Wei F, Wang H, Zhang G, Huang Y, Zhang Y. Grafting SiO2 nanoparticles on polyvinyl alcohol fibers to enhance the interfacial bonding strength with cement. Compos B Eng 2019;162:500–7.
[199] Rezaie AB, Liebscher M, Ranjbarian M, Simon F, Zimmerer C, Drechsler A, Frenzel R, Synytska A, Mechtcherine V. Enhancing the interfacial bonding between PE fibers and cementitious matrices through polydopamine surface modification. Compos B Eng 2021;217:108817.
[200] Chun B, Yoo DY, Banthia N. Achieving slip-hardening behavior of sanded straight steel fibers in ultra-high-performance concrete. Cement Concr Compos 2020: 103669.
[201] Yoo D-Y, Oh T, Chun B. Highly ductile ultra-rapid-hardening mortar containing oxidized polyethylene fibers. Construct Build Mater 2021;277:122317.
[202] Ženíšek M, Vlach T, Řepka J, Pavlů T. Segregation of steel fibres of UHPFRC. In: Solid state phenomena. Trans Tech Publ; 2018.
[203] Bensted J. Effects of the clinker-gypsum grinding temperature upon early hydration of Portland cement. Cement Concr Res 1982;12(3):341–8.
[204] Xie T, Fang C, Ali MM, Visintin P. Characterizations of autogenous and drying shrinkage of ultra-high performance concrete (UHPC): an experimental study. Cement Concr Compos 2018;91:156–73.
[205] Yang R, Yu R, Shui Z, Gao X, Xiao X, Zhang X, Wang Y, He Y. Low carbon design of an ultra-high performance concrete (UHPC) incorporating phosphorous slag. J Clean Prod 2019;240:118157.
[206] Teng L, Meng W, Khayat KH. Rheology control of ultra-high-performance concrete made with different fiber contents. Cement Concr Res 2020;138:106222.
[207] Huang H, Ye G. Examining the "time-zero" of autogenous shrinkage in high/ultra-high performance cement pastes. Cement Concr Res 2017;97:107–14.
[208] Ghafari E, Ghahari SA, Costa H, Júlio E, Portugal A, Durães L. Effect of supplementary cementitious materials on autogenous shrinkage of ultra-high performance concrete. Construct Build Mater 2016;127:43–8.
[209] De Sensale GR, Ribeiro AB, Gonçalves A. Effects of RHA on autogenous shrinkage of Portland cement pastes. Cement Concr Compos 2008;30(10):892–7.
[210] Li P, Brouwers H, Chen W, Yu Q. Optimization and characterization of high-volume limestone powder in sustainable ultra-high performance concrete. Construct Build Mater 2020;242:118112.
[211] Justs J, Wyrzykowski M, Bajare D, Lura P. Internal curing by superabsorbent polymers in ultra-high performance concrete. Cement Concr Res 2015;76:82–90.
[212] Anshuang S, Ling Q, Shoujie Z, Jiayang Z, Zhaoyu L. Effects of shrinkage reducing agent and expansive admixture on the volume deformation of ultrahigh performance concrete. Adv. Mater. Sci. Eng. 2017;2017:6384859.
[213] Zhibin Z, Lingling X, Minshu T. Synergistic effect of MgO-based expansive agent and shrinkage-reducing admixture on compensating the shrinkage of cementitious materials, vol. 262. Special Publication; 2009. p. 395–406.
[214] Shen P, Lu L, He Y, Wang F, Lu J, Zheng H, Hu S. Investigation on expansion effect of the expansive agents in ultra-high performance concrete. Cement Concr Compos 2020;105:103425.
[215] Tazawa E-i, Miyazawa S, Kasai T. Chemical shrinkage and autogenous shrinkage of hydrating cement paste. Cement Concr Res 1995;25(2):288–92.
[216] Henkensiefken R, Bentz D, Nantung T, Weiss J. Volume change and cracking in internally cured mixtures made with saturated lightweight aggregate under sealed and unsealed conditions. Cement Concr Compos 2009;31(7):427–37.
[217] Lyu Z, Guo Y, Chen Z, Shen A, Qin X, Yang J, Zhao M, Wang Z. Research on shrinkage development and fracture properties of internal curing pavement concrete based on humidity compensation. Construct Build Mater 2019;203: 417–31.
[218] Yang L, Shi C, Wu Z. Mitigation techniques for autogenous shrinkage of ultra-high-performance concrete–A review. Compos B Eng 2019:107456.
[219] Lyu Z, Shen A, Mo S, Chen Z, He Z, Li D, Qin X. Life-cycle crack resistance and micro characteristics of internally cured concrete with superabsorbent polymers. Construct Build Mater 2020;259:119794.
[220] Lyu Z, Shen A, He Z, Wang W, Mo S, Chen Z, Qin X. Absorption characteristics and shrinkage mitigation of superabsorbent polymers in pavement concrete. Int J Pavement Eng 2020:1–15.
[221] Sun B, Wu H, Song W, Li Z, Yu J. Design methodology and mechanical properties of Superabsorbent Polymer (SAP) cement-based materials. Construct Build Mater 2019;204:440–9.
[222] Liu J, Farzadnia N, Khayat KH, Shi C. Effects of SAP characteristics on internal curing of UHPC matrix. Construct Build Mater 2021;280:122530.
[223] Liu J, Farzadnia N, Shi C, Ma X. Shrinkage and strength development of UHSC incorporating a hybrid system of SAP and SRA. Cement Concr Compos 2019;97: 175–89.
[224] Liu J, Shi C, Farzadnia N, Ma X. Effects of pretreated fine lightweight aggregate on shrinkage and pore structure of ultra-high strength concrete. Construct Build Mater 2019;204:276–87.
[225] Ferrara L, Ferreira SR, della Torre M, Krelani V, de Silva FA, Toledo Filho RD. Effect of cellulose nanopulp on autogenous and drying shrinkage of cement based composites. In: Nanotechnology in construction. Springer; 2015. p. 325–30.
[226] Hisseine OA, Soliman NA, Tolnai B, Tagnit-Hamou A. Nano-engineered ultra-high performance concrete for controlled autogenous shrinkage using nanocellulose. Cement Concr Res 2020;137:106217.
[227] Li S, Cheng S, Mo L, Deng M. Effects of steel slag powder and expansive agent on the properties of ultra-high performance concrete (UHPC): based on a case study. Materials 2020;13(3):683.
[228] Wehbe Y, Ghahremaninezhad A. Combined effect of shrinkage reducing admixtures (SRA) and superabsorbent polymers (SAP) on the autogenous shrinkage, hydration and properties of cementitious materials. Construct Build Mater 2017;138:151–62.
[229] Zuo W, Feng P, Zhong P, Tian Q, Gao N, Wang Y, Yu C, Miao C. Effects of novel polymer-type shrinkage-reducing admixture on early age autogenous deformation of cement pastes. Cement Concr Res 2017;100:413–22.
[230] Soliman A, Nehdi M. Effects of shrinkage reducing admixture and wollastonite microfiber on early-age behavior of ultra-high performance concrete. Cement Concr Compos 2014;46:81–9.
[231] Graybeal BA. Characterization of the behavior of ultra-high performance concrete. Doctoral dissertation. 2005.
[232] Cheng Y-H, Zhu B-L, Yang S-H, Tong B-Q. Design of concrete mix proportion based on particle packing voidage and test research on compressive strength and elastic modulus of concrete. Materials 2021;14(3):623.
[233] Van Der Putten J, Dils J, Minne P, Boel V, De Schutter G. Determination of packing profiles for the verification of the compressible packing model in case of UHPC pastes. Mater Struct 2017;50(2):1–14.
[234] Powers TC. A discussion of cement hydration in relation to the curing of concrete. In: Highway research board proceedings; 1948.
[235] Mostafa SA, Faried AS, Farghali AA, El-Deeb MM, Tawfik TA, Majer S, Abd Elrahman M. Influence of nanoparticles from waste materials on mechanical properties, durability and microstructure of UHPC. Materials 2020;13(20):4530.
[236] Meng W, Khayat KH. Effect of graphite nanoplatelets and carbon nanofibers on rheology, hydration, shrinkage, mechanical properties, and microstructure of UHPC. Cement Concr Res 2018;105:64–71.
[237] Norhasri MM, Hamidah M, Fadzil AM. Inclusion of nano metaclayed as additive in ultra high performance concrete (UHPC). Construct Build Mater 2019;201:590–8.
[238] Liu C, He X, Deng X, Wu Y, Zheng Z, Liu J, Hui D. Application of nanomaterials in ultra-high performance concrete: a review. Nanotechnol Rev 2020;9(1):1427–44.
[239] Wu Z, Shi C, Khayat KH. Multi-scale investigation of microstructure, fiber pullout behavior, and mechanical properties of ultra-high performance concrete with nano-CaCO3 particles. Cement Concr Compos 2018;86:255–65.
[240] Aïtcin P-C. High performance concrete. CRC press; 1998.
[241] Shen P, Lu L, He Y, Wang F, Hu S. The effect of curing regimes on the mechanical properties, nano-mechanical properties and microstructure of ultra-high performance concrete. Cement Concr Res 2019;118:1–13.
[242] Zhang Y, Li X, Zhu Y, Shao X. Experimental study on flexural behavior of damaged reinforced concrete (RC) beam strengthened by toughness-improved ultra-high performance concrete (UHPC) layer. Compos B Eng 2020;186:107834.
[243] Lantsoght EO. How do steel fibers improve the shear capacity of reinforced concrete beams without stirrups? Compos B Eng 2019;175:107079.
[244] Kang ST, Lee BY, Kim J-K, Kim YY. The effect of fibre distribution characteristics on the flexural strength of steel fibre-reinforced ultra high strength concrete. Construct Build Mater 2011;25(5):2450–7.
[245] Teng L, Huang H, Du J, Khayat K. Prediction of fiber orientation and flexural performance of UHPC based on suspending mortar rheology and casting method. Cement Concr Compos 2021;122:104142.
[246] Meng W, Khayat KH, Bao Y. Flexural behaviors of fiber-reinforced polymer fabric reinforced ultra-high-performance concrete panels. Cement Concr Compos 2018; 93:43–53.
[247] Martinie L, Roussel N. Simple tools for fiber orientation prediction in industrial practice. Cement Concr Res 2011;41(10):993–1000.
[248] Swamy R. Fibre reinforcement of cement and concrete. Matériaux et Construction 1975;8(3):235–54.
[249] Banthia N, Trottier J-F. Concrete reinforced with deformed steel fibers, part I: bond-slip mechanisms. Mater. J. 1994;91(5):435–46.
[250] Armelin HS, Banthia N. Predicting the flexural postcracking performance of steel fiber reinforced concrete from the pullout of single fibers. Mater. J. 1997;94(1): 18–31.
[251] Svec O, Skocek J, Stang H, Olesen JF, Thrane L. Application of the fluid dynamics model to the field of fibre reinforced self-compacting concrete. In: Proceedings of the numerical modeling strategies for sustainable concrete structures (NMSSC); 2012. p. 1–9.
[252] Song Q, Yu R, Shui Z, Wang X, Rao S, Lin Z. Optimization of fibre orientation and distribution for a sustainable ultra-high performance fibre reinforced concrete (UHPFRC): experiments and mechanism analysis. Construct Build Mater 2018; 169:8–19.

[253] Song Q, Yu R, Shui Z, Wang X, Rao S, Lin Z, Wang Z. Key parameters in optimizing fibres orientation and distribution for ultra-high performance fibre reinforced concrete (UHPFRC). Construct Build Mater 2018;188:17–27.
[254] Huang H, Su A, Gao X, Yang Y. Influence of formwork wall effect on fiber orientation of UHPC with two casting methods. Construct Build Mater 2019;215:310–20.
[255] Qureshi TS, Panesar DK. Nano reinforced cement paste composite with functionalized graphene and pristine graphene nanoplatelets. Compos B Eng 2020;197:108063.
[256] Yoo D-Y, Kim S-W, Park J-J. Comparative flexural behavior of ultra-high-performance concrete reinforced with hybrid straight steel fibers. Construct Build Mater 2017;132:219–29.
[257] Wille K, El-Tawil S, Naaman AE. Properties of strain hardening ultra high performance fiber reinforced concrete (UHP-FRC) under direct tensile loading. Cement Concr Compos 2014;48:53–66.
[258] El-Hacha R, Chen D. Behaviour of hybrid FRP–UHPC beams subjected to static flexural loading. Compos B Eng 2012;43(2):582–93.
[259] Ren L, Fang Z, Wang K. Design and behavior of super-long span cable-stayed bridge with CFRP cables and UHPC members. Compos B Eng 2019;164:72–81.
[260] Meng W, Khayat KH. Experimental and numerical studies on flexural behavior of ultrahigh-performance concrete panels reinforced with embedded glass fiber-reinforced polymer grids. Transport Res Rec 2016;2592(1):38–44.
[261] Soltan DG, Li VC. Nacre-inspired composite design approaches for large-scale cementitious members and structures. Cement Concr Compos 2018;88:172–86.
[262] Cao Y, Liu G, Brouwers H, Yu Q. Enhancing the low-velocity impact resistance of ultra-high performance concrete by an optimized layered-structure concept. Compos B Eng 2020;200:108221.
[263] Cao Y, Li P, Brouwers H, Sluijsmans M, Yu Q. Enhancing flexural performance of ultra-high performance concrete by an optimized layered-structure concept. Compos B Eng 2019;171:154–65.
[264] Zhang G, Wu C, Hou D, Yang J, Sun D, Zhang X. Effect of environmental pH values on phase composition and microstructure of Portland cement paste under sulfate attack. Compos B Eng 2021;216:108862.
[265] Tam CM, Tam VW, Ng KM. Assessing drying shrinkage and water permeability of reactive powder concrete produced in Hong Kong. Construct Build Mater 2012;26(1):79–89.
[266] Roux N, Andrade C, Sanjuan M. Experimental study of durability of reactive powder concretes. J Mater Civ Eng 1996;8(1):1–6.
[267] Franke L, Schmidt H, Deckelmann G. Behavior of ultra-high performance concrete with respect to chemical attack. In: Proceedings of the 2nd international symposium on ultra-high performance concrete. Germany: Kassel; 2008.
[268] Piérard J, Dooms B, Cauberg N. Durability evaluation of different types of UHPC. In: Proceedings of the RILEM-fib-AFGC international symposium on ultra-high performance fiber-reinforced concrete; 2013.
[269] Chen Y, Yu R, Wang X, Chen J, Shui Z. Evaluation and optimization of ultra-high performance concrete (UHPC) subjected to harsh ocean environment: towards an application of layered double hydroxides (LDHs). Construct Build Mater 2018;177:51–62.
[270] Heinz D, Dehn F, Urbonas L. Fire resistance of ultra high performance concrete (UHPC)-Testing of laboratory samples and columns under load. In: International symposium on ultra high performance concrete. Kassel Germany; 2004.
[271] Ahlborn TM, Misson DL, Peuse EJ, Gilbertson CG. Durability and strength characterization of ultra-high performance concrete under variable curing regimes. In: Fehling E, Schmidt M, Stürwald S, editors. Proc. 2nd Int. Symp. On ultra high performance concrete. Germany: Kassel; 2008.
[272] Scheydt JC, Muller S. Microstructure of ultra high performance concrete (UHPC) and its impact on durability. In: Proceedings of the 3rd international symposium on UHPC and nanotechnology for high performance construction materials. Germany: Kassel; 2012.
[273] Smarzewski P, Barnat-Hunek D. Effect of fiber hybridization on durability related properties of ultra-high performance concrete. Int. J. Concr. Struct. Mater. 2017;11(2):315–25.
[274] Liu S, Sun W, Lin W, Lai J. Preparation and durability of a high performance concrete with natural ultra-fine particles. Guisuanyan Xuebao 2003;31:1080–5.
[275] Pease B, Geiker M, Stang H, Weiss J. The design of an instrumented rebar for assessment of corrosion in cracked reinforced concrete. Mater Struct 2011;44(7):1259–71.
[276] Rajczakowska M, Habermehl-Cwirzen K, Hedlund H, Cwirzen A. Autogenous self-healing: a better solution for concrete. J Mater Civ Eng 2019;31(9):03119001.
[277] Beglarigale A, Eyice D, Tutkun B, Yazıcı H. Evaluation of enhanced autogenous self-healing ability of UHPC mixtures. Construct Build Mater 2021;280:122524.
[278] Deschenes Jr RA. Mitigation and evaluation of alkali-silica reaction (ASR) and freezing and thawing in concrete transportation structures. 2017.
[279] Rachida I, Cyr M, Tagnit-Hamou A. Use of waste glass in cement-based materials. Déchets, Sciences et Techniques 2010;57:10.
[280] Mazzacane P, Ricciotti R, Teply F, Tollini E, Corvez D. MUCEM: the builder's perspective. Proceedings UHPFRC 2013:3–16.
[281] Aubry S, Bompas P, Vaudeville B, Corvez D, Lagrange T, Mazzacane P, Brizou A. A UHPFRC cladding challenge: the fondation Louis Vuitton pour la création" Iceberg. In: 2nd RILEM-fib-AFGC international symposium on ultra-high performance fibre-reinforced concrete; 2013.
[282] Mazzacane P, Ricciotti R, Lamoureux G, Corvez D. Roofing of the stade jean Bouin in UHPFRC. In: Proceedings of international symposium on ultra-high performance fibre-reinforced concrete; 2013.
[283] Muttoni A, Brauen U, Jaquier J-L, Moullet D. A new roof for the olympic museum at Lausanne, Switzerland. In: Proceedings of international symposium on ultra-high performance fiber-reinforced concrete; 2013.
[284] Menétrey P. UHPFRC cladding for the Qatar national museum. In: Proceedings of international symposium on ultra-high performance fiber-reinforced concrete; 2013. Marseille, France.
[285] Gaudillière N, Duballet R, Bouyssou C, Mallet A, Roux P, Zakeri M, Dirrenberger J. Large-scale additive manufacturing of ultra-high-performance concrete of integrated formwork for truss-shaped pillars. In: Robotic fabrication in architecture, art and design. Springer; 2018.
[286] Graybeal BA. Structural behavior of ultra-high performance concrete prestressed I-girders. United States: Federal Highway Administration; 2006.
[287] Graybeal BA. Structural behavior of a 2nd generation ultra-high performance concrete pi-girder. United States: Federal Highway Administration; 2009.
[288] Aaleti S, Petersen B, Sritharan S. Design guide for precast UHPC waffle deck panel system, including connections. United States: Federal Highway Administration; 2013.
[289] Zhou M, Lu W, Song J, Lee GC. Application of ultra-high performance concrete in bridge engineering. Construct Build Mater 2018;186:1256–67.
[290] Graybeal B. Design and construction of field-cast UHPC connections. United States: Federal Highway Administration; 2014.
[291] Wibowo H, Sritharan S. Use of ultra-high-performance concrete for bridge deck overlays. United States: Federal Highway Administration; 2018.
[292] Haber ZB, Munoz JF, De la Varga I, Graybeal BA. Bond characterization of UHPC overlays for concrete bridge decks: laboratory and field testing. Construct Build Mater 2018;190:1056–68.
[293] Kennedy D, Habel K, Fraser G. Ultra high-performance concrete column jacket retrofit for the mission bridge. In: 11th Canadian conference on earthquake engineering; 2015.
[294] Gamarra J. Potential application of ultra-high performance fiber-reinforced concrete with wet-mix shotcrete system in tunneling. Doctoral dissertation. 2016.
[295] Sritharan S, Schmitz GM. Design of tall wind turbine towers utilizing UHPC. In: 2nd international symposium on ultra-high performance fibre-reinforced concrete. Marseille, France: UHPFRC; 2013.
[296] Khan MU, Ahmad S, Naqvi AA, Al-Gahtani HJ. Shielding performance of heavy-weight ultra-high-performance concrete against nuclear radiation. Prog Nucl Energy 2020;130:103550.
[297] Ahmad S, Mohaisen KO, Adekunle SK, Al-Dulaijan SU, Maslehuddin M. Influence of admixing natural pozzolan as partial replacement of cement and microsilica in UHPC mixtures. Construct Build Mater 2019;198:437–44.
[298] Zhang D, Tan KH, Dasari A, Weng Y. Effect of natural fibers on thermal spalling resistance of ultra-high performance concrete. Cement Concr Compos 2020:103512.